

Experimental Verification of the Behavioral Foundation of Bacterial Transport Parameters Using Microfluidics

Tanvir Ahmed and Roman Stocker

Ralph M. Parsons Laboratory, Department of Civil and Environmental Engineering, Massachusetts Institute of Technology, Cambridge, Massachusetts

ABSTRACT We present novel microfluidic experiments to quantify population-scale transport parameters (chemotactic sensitivity χ_0 and random motility μ) of a population of bacteria. Previously, transport parameters have been derived theoretically from single-cell swimming behavior using probabilistic models, yet the mechanistic foundations of this upscaling process have not been verified experimentally. We designed a microfluidic capillary assay to generate and accurately measure gradients of chemoattractant (α -methylaspartate) while simultaneously capturing the swimming trajectories of individual *Escherichia coli* bacteria using videomicroscopy and cell tracking. By measuring swimming speed and bias in the swimming direction of single cells for a range of chemoattractant concentrations and concentration gradients, we directly computed the chemotactic velocity V_C and the associated chemotactic sensitivity χ_0 . We then show how μ can also be readily determined using microfluidics but that a population-scale microfluidic approach is experimentally more convenient than a single-cell analysis in this case. Measured values of both χ_0 [$(12.4 \pm 2.0) \times 10^{-4} \text{ cm}^2 \text{ s}^{-1}$] and μ [$(3.3 \pm 0.8) \times 10^{-6} \text{ cm}^2 \text{ s}^{-1}$] are comparable to literature results. This microscale approach to bacterial chemotaxis lends experimental support to theoretical derivations of population-scale transport parameters from single-cell behavior. Furthermore, this study shows that microfluidic platforms can go beyond traditional chemotaxis assays and enable the quantification of bacterial transport parameters.

INTRODUCTION

Chemotaxis is the ability of cells to detect and respond to a gradient in chemical concentration. The motility and chemotaxis phenotypes have significant impact in a wide range of fields, including reproduction science (1,2), biofilm formation (3,4), contaminant bioremediation (5–7), disease pathogenesis (8–10), and nutrient cycling in the ocean (11–15). A quantification of chemotactic motility is therefore essential to predict the ability of a bacterial population to disperse and migrate in the presence of chemical gradients.

Bacterial motility is often described as a three-dimensional (3D) random walk (16). For the enteric bacterium *Escherichia coli*, 3D tracking (17) revealed that the random walk is composed of nearly straight segments (“runs”) interrupted by rapid changes in direction (“tumbles”). When bacteria experience favorable chemical gradients, tumbles are suppressed (18,19), resulting in a net chemotactic drift with velocity V_C toward an attractant or away from a repellent. At the population scale, this behavior has been characterized by a phenomenological model for the flux of cells J proposed by Keller and Segel (20), which in one dimension (x) reads

$$J = -\mu \frac{\partial B}{\partial x} + V_C B. \quad (1)$$

Here, $B(x,t)$ is the concentration of bacteria, t is time, and μ is the random motility coefficient, measuring the diffusivity of a population of bacteria resulting from their random walk behavior. Coupled with the conservation equation $\partial B/\partial t = -\partial J/\partial x$, Eq. 1 gives an advection-diffusion equation for the bacterial population, known as the bacterial transport equation:

$$\frac{\partial B}{\partial t} = \frac{\partial}{\partial x} \left(\mu \frac{\partial B}{\partial x} \right) - \frac{\partial}{\partial x} (V_C B). \quad (2)$$

In the absence of chemoattractants, $V_C = 0$ and Eq. 2 reduces to the diffusion equation. When a chemoattractant is present, the chemotactic velocity V_C depends on the chemoattractant concentration gradient and hence is not an intrinsic property of a bacterium-chemoattractant pair. Instead, such a role is played by the chemotactic sensitivity coefficient χ_0 , expressing the strength of attraction of a population to a given chemical. The relation between V_C and χ_0 is discussed below. It follows from Eq. 2 that knowledge of μ and χ_0 enables one to predict bacterial transport in any given concentration field. Conversely, observed bacterial distributions can be used to determine μ and χ_0 by fitting Eq. 2.

A wide range of chemotaxis assays has been developed to measure the strength of attraction of a bacterial population to a given chemical. The classic “capillary assay” (21) is the most widespread, due to its simplicity. However, capillary assays are not conducive to the measurement of transport parameters (22,23), as chemoattractant gradients are exceedingly difficult to quantify and can be easily perturbed even by minor residual flows (24). Furthermore, the need for plate-counting considerably increases processing time and reduces accuracy. Quantification of transport parameters has typically relied on

Submitted April 3, 2008, and accepted for publication July 11, 2008.

Address reprint requests to Roman Stocker, Civil and Environmental Engineering, Massachusetts Institute of Technology, 15 Vassar Street, Building 48, Room 335, Cambridge, MA 02139. Tel: 617-253-3726; E-mail: romans@mit.edu.

Editor: Jason M. Haugh.

© 2008 by the Biophysical Society
0006-3495/08/11/4481/13 \$2.00

doi: 10.1529/biophysj.108.134510

Translational Repression Contributes Greater Noise to Gene Expression than Transcriptional Repression

Michał Komorowski,[†] Jacek Miękiś,[†] and Andrzej M. Kierzek^{†*}

[†]Institute of Applied Mathematics and Mechanics, University of Warsaw, Warsaw, Poland; and ^{*}Faculty of Health and Medical Sciences, University of Surrey, Guildford, United Kingdom

ABSTRACT Stochastic effects in gene expression may result in different physiological states of individual cells, with consequences for pathogen survival and artificial gene network design. We studied the contributions of a regulatory factor to gene expression noise in four basic mechanisms of negative gene expression control: 1), transcriptional regulation by a protein repressor, 2), translational repression by a protein; 3), transcriptional repression by RNA; and 4), RNA interference with the translation. We investigated a general model of a two-gene network, using the chemical master equation and a moment generating function approach. We compared the expression noise of genes with the same effective transcription and translation initiation rates resulting from the action of different repressors, whereas previous studies compared the noise of genes with the same mean expression level but different initiation rates. Our results show that translational repression results in a higher noise than repression on the promoter level, and that this relationship does not depend on quantitative parameter values. We also show that regulation of protein degradation contributes more noise than regulated degradation of mRNA. These are unexpected results, because previous investigations suggested that translational regulation is more accurate. The relative magnitude of the noise introduced by protein and RNA repressors depends on the protein and mRNA degradation rates, and we derived expressions for the threshold below which the noise introduced by a protein repressor is higher than the noise introduced by an RNA repressor.

INTRODUCTION

It was first postulated by theory (1–3), and later confirmed by numerous experiments (4–10), that a low number of molecules taking part in the regulation of gene expression results in significant random fluctuations in this process, and that the magnitude of random fluctuations depends on the mechanism of gene regulation (11–14). It was also demonstrated that stochastic effects in gene expression may result in different physiological states of individual cells, leading to heterogeneous cellular populations, with important consequences for pathogen survival strategies (15,16) and the design of artificial gene networks applicable in biotechnology and gene therapy (17). These results prompted numerous studies about the origins of stochastic fluctuations in gene expression processes (10,14,18–21), and one of the most important advances was the development of experimental methods allowing a determination of extrinsic and intrinsic components of the total gene expression noise (9,19). Intrinsic noise is measured as the stochastic variability between two identical genes expressed in the same single cell. It represents sources of noise located within transcriptional and translational machineries of a single gene, such as DNA conformational changes and the movement of polymerases and ribosomes during elongation processes.

The remaining component of total gene expression noise is referred to as the extrinsic noise, and represents fluctuations in a single gene expression attributable to random changes in concentrations, states, and locations of molecules required for the expression of two identical genes in the same single cell. Therefore, extrinsic noise is determined by random fluctuations in the quantity of active polymerases, ribosomes, and transcription and translation factors available for a single gene located in a single cell. Another important result, obtained first as a theoretical prediction and subsequently confirmed by experimental studies, is the relationship between gene expression noise and the frequency of transcription and translation initiation (5,11,12). If genes are expressed at the same low level, where stochastic fluctuations are significant, the gene expressed with a lower translation initiation frequency exhibits lower variance in the number of protein molecules. These results imply an evolutionary tradeoff between the accurate and the energetically efficient gene expression control. The gene can be expressed at a very low level without large stochastic fluctuations if it is down-regulated at the translation level. This, however, means that a lot of mRNA molecules are synthesized but not translated, which effectively raises the number of ATP molecules consumed to produce a single protein molecule.

We studied the contributions of a regulatory factor produced by one gene to the variance in the number of protein molecules produced by another gene. Therefore, we studied the contributions of a particular regulatory factor to the extrinsic noise of gene expression. We focused on regulatory factors that decrease the activity of a regulated

Submitted January 24, 2008, and accepted for publication September 22, 2008.

*Correspondence: a.kierzek@surrey.ac.uk

Michał Komorowski's present address is the Dept. of Statistics and Systems Biology Centre, University of Warwick, Coventry CV4 7AL, UK.

Editor: Herbert Levine.

© 2009 by the Biophysical Society
0006-3495/09/01/0372/13 \$2.00

doi: 10.1016/j.bpj.2008.09.052

Dynamical Analysis on Gene Activity in the Presence of Repressors and an Interfering Promoter

Hiizu Nakanishi,^{*†} Namiko Mitarai,[†] and Kim Sneppen^{*}

^{*}Niels Bohr Institute, Copenhagen, Denmark; and [†]Department of Physics, Kyushu University, Fukuoka, Japan

ABSTRACT Transcription is regulated through interplay among transcription factors, an RNA polymerase (RNAP), and a promoter. Even for a simple repressive transcription factor that disturbs promoter activity at initial binding of RNAP, its repression level is not determined solely by the dissociation constant of transcription factor but is sensitive to timescales of processes in RNAP. We first analyze the promoter activity under strong repression by a slow binding repressor, in which case transcription events occur in bursts, followed by long quiescent periods while a repressor binds to the operator; the number of transcription events, bursting, and quiescent times are estimated by reaction rates. We then examine interference effect from an opposing promoter, using the correlation function of initiation events for a single promoter. The interference is shown to de-repress the promoter because RNAPs from the opposing promoter most likely encounter the repressor and remove it in case of strong repression. This de-repression mechanism should be especially prominent for the promoters that facilitate fast formation of open complex with the repressor whose binding rate is slower than $\sim 1/s$. Finally, we discuss possibility of this mechanism for high activity of promoter PR in the hyp-mutant of λ -phage.

INTRODUCTION

The regulation of the activity of a particular gene involves a complex interplay between a promoter, an RNA polymerase (RNAP), and one or several transcription factors (TF) (1,2). Ignoring the internal dynamics associated with transcription initiation, the probability for obtaining a successful RNAP elongation initiation can be estimated from an equilibrium unbinding ratio of TF (3,4). When internal steps in transcription initiations become sizeable we need to consider the race between these steps and the kinetics of TF binding.

The binding/unbinding rates of TF to bind to an operator is critically influenced by competitive nonspecific bindings (5,6). Recent measurements of in vivo dynamics in an *Escherichia coli* cell finds that a single Lac repressor needs between 60 and 360 s to locate its operator (6). For TFs whose copy number is ~ 10 – 100 per cell, a cleared operator can remain free for up to ~ 30 s. In comparison, RNAP transcription initiation rates varies considerably, and can be as fast as 1.8 transcription initiations per s for a certain ribosomal promoter (7). Therefore, there is room for effects associated to the race between first bindings of a TF or an RNAP once the promoter is cleared.

In a number of both prokaryotic and eukaryotic systems, the promoter activity are not only influenced by TF, but are also modulated by interfering promoters (8–15). For example, the regulation between lytic and lysogenic maintenance promoters in the P2 class of bacteriophages involves transcription interferences (TI) as well as TFs that repress the promoter activities (11). In λ -phages, the initial lysis-lysogeny decision is modulated by TI between the promoter PRE activated by CII and the promoter PR repressed by CI.

Dodd et al. (15) presented a framework to deal with TI and multiple TFs, using an assumption about fast equilibrium reactions of TF-binding and closed complex formation. In this article, we develop a formalism that deals with the competition between timescales of TF binding/unbinding and transcription initiation process, and examine the effect of interference.

Fig. 1 shows a single promoter pS with an operator site for a repressive TF (*left panel*), and with a convergent promoter pA (*right panel*). For both cases, we illustrate the three basic steps of transcription initiation: 1), RNAP reversible binding to form a closed complex; 2), irreversible transition to open complex; and 3), initiation of transcription elongation. The rates for these three steps are promoter-dependent (16–18). As for the initial binding, given the fact that the maximum activity for ribosomal promoters reaches 1.8 transcription events per s (7), the time needed for an RNAP to diffuse to a promoter cannot be longer than ~ 0.5 s. Regarding the later steps where RNAP forms an open complex and subsequently initiates transcription to leave the promoter, their timescales may vary a great deal from one promoter to another (19–23).

In the following, we will investigate in detail how these timescales play together to determine the extent to which a promoter is sensitive to repressors and to clearance due to the interference by elongating RNAPs from other promoters (note that a Java applet for the promoter model with a transcription factor is available at <http://cmol.nbi.dk/models/dynamtrans/dynamtrans.html>).

MODELS

We study the promoter activity under influence of TF and TI based on mathematical analysis on simple models of promoter in the following three levels. Our goal is to understand regulation of the three-step model for

Submitted March 7, 2008, and accepted for publication July 17, 2008.

Address reprint requests to Hiizu Nakanishi, Tel.: 81-92-642-2568; E-mail: nakanishi@phys.kyushu-u.ac.jp.

Editor: Alexander Mogilner.

© 2008 by the Biophysical Society
0006-3495/08/11/4228/13 \$2.00

doi: 10.1529/biophysj.108.132894

Site-Specific Immobilization and Micrometer and Nanometer Scale Photopatterning of Yellow Fluorescent Protein on Glass Surfaces

Nicholas P. Reynolds,[†] Jaimey D. Tucker,[‡] Paul A. Davison,[‡] John A. Timney,[‡] C. Neil Hunter,[‡] and Graham J. Leggett^{*†}

Department of Chemistry, University of Sheffield, Brook Hill, Sheffield S3 7HF, U.K., and Department of Molecular Biology and Biotechnology, University of Sheffield, Western Bank, Sheffield S10 2TN, U.K.

Received October 7, 2008; E-mail: graham.leggett@sheffield.ac.uk

The development of methods for molecular patterning with nanoscale spatial resolution remains a significant challenge in the burgeoning field of bionanotechnology. While there has been a great deal of progress in the development of techniques based on scanning probe microscopy, such as dip-pen nanolithography,^{1–6} nanoshaving/grafting,⁷ and near-field optical methods,^{8–10} much work has focused on nucleic acids, and there are fewer reports of protein patterning. Moreover, much work has also utilized self-assembled monolayers (SAMs) of alkanethiols on gold as templates for molecular patterning. In addition to a limited stability, they suffer the disadvantage that gold quenches optical activity, rendering the interrogation of biomolecules by spectroscopic techniques more difficult. From the perspective of applications in biology, nanostructures formed on oxide surfaces are particularly attractive,¹¹ and the oxide of choice would be, in many cases, glass. There have been comparatively few attempts to fabricate nanostructures on silicon dioxide, with the development of constructive nanolithography by Sagiv and co-workers being the most extensive effort to date in this direction.^{12,13}

In a previous study, it was demonstrated that UV exposure of tri(ethylene glycol) terminated alkanethiol SAMs caused their degradation to yield surface aldehyde groups, which covalently bound amines and proteins.¹⁴ Here we report a development that should facilitate the nanometer-scale patterning of any histidine-tagged protein on glass. It is shown first, that an oligo(ethylene glycol) (OEG) terminated siloxane monolayer on glass may be degraded by UV light to yield aldehyde groups; second, that these may be used to immobilize nitrilo(triacetic acid) terminated amines, facilitating site-specific immobilization of His-tagged proteins;⁶ and third, that combination of this method with near-field exposure yields sub-200 nm structures that may be imaged by confocal microscopy to yield diffraction-limited images.

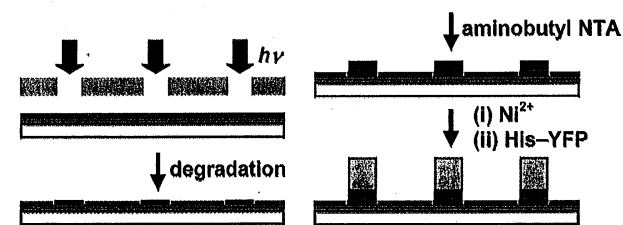


Figure 1. Schematic diagram representing the process used to immobilize His-YFP.

The method is shown schematically in Figure 1. A glass surface was immersed in a solution of mercaptopropyltrimethoxysilane (MPTMS) in tetrahydrofuran yielding a mercaptosilane-function-

alized substrate that was then derivatized with methyl-PEO₁₂-maleimide (PEO = poly(ethylene oxide)), yielding a protein-resistant surface. The sample was exposed to UV light from a frequency-doubled argon ion laser (244 nm) through a mask or, for nanometer scale patterning, using a scanning near-field optical microscope. In exposed areas, EO groups were degraded to yield aldehydes. Samples were then placed in a solution of *N*-[5-(3'-maleimidopropylamido)-1-carboxypentyl] iminodiacetic acid in deionized water, yielding a nitrilotriacetic acid terminated surface which, following exposure to a solution of nickel ions was able to bind proteins. The protein used here was histidine-tagged yellow fluorescent protein (His-YFP, see Supporting Information for details of its preparation).

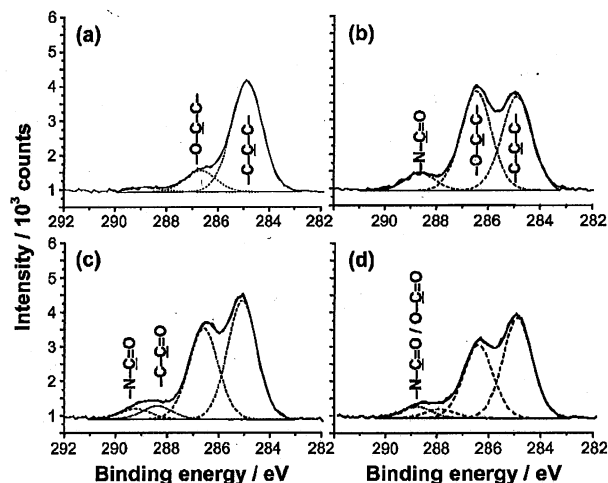


Figure 2. C1s XPS spectra of MPTMS films on glass: (a) virgin monolayer; (b) after derivatization with methyl-PEO₁₂-maleimide; (c) after subsequent exposure to UV light (7.6 J cm⁻²); and (d) after further derivatization with *N*-(5-amino-1-carboxypentyl)iminodiacetic acid.

X-ray photoelectron spectroscopy (XPS) was used to characterize the surface attachment chemistry (Figure 2). The C1s spectrum of the MPTMS film (Figure 2a) exhibited a peak at 285 eV corresponding to the aliphatic carbon atoms in the propyl chain, together with a small ether peak, attributed to unreacted methoxy groups. Following derivatization with methyl-PEO₁₂-maleimide, the ether component became the dominant one in the spectrum (Figure 2b) and a peak was observed at 288.9 eV due to the imide carbon atoms. Exposure to 7.6 J cm⁻² UV light (Figure 2c) led to a reduction in the intensity of the ether peak, and the appearance of a new peak 288.2 eV attributed to the formation of aldehydes. These data indicate that the PEO functionalized siloxane film undergoes a similar degradation process to the one reported previously for OEG functionalized alkanethiol SAMs.¹⁴ Doubling the exposure yielded

[†] Department of Chemistry.

[‡] Department of Molecular Biology and Biotechnology.

Selective Recognition of Protein Tetraserine Motifs with a Cell-Permeable, Pro-fluorescent Bis-boronic Acid

Tiffany L. Halo,[†] Jacob Appelbaum,[§] Elissa M. Hobert,[†] Daniel M. Balkin,[§] and Alanna Schepartz^{*,†,‡}

Departments of Chemistry and Molecular, Cellular, and Developmental Biology, Yale University, New Haven, Connecticut 06520, and Department of Cell Biology, Yale University School of Medicine, New Haven, Connecticut 06510

Received October 6, 2008; E-mail: alanna.schepartz@yale.edu

There is considerable interest in novel biomolecule imaging tools that avoid the use of fluorescent proteins.^{1–3} One widely used class of such reagents are “pro-fluorescent” biarsenical dyes such as FLAsH,⁴ ReAsH,⁵ CrAsH,⁶ and Cy3As.⁷ These cell-permeable molecules selectively label recombinant proteins containing a linear⁴ or split⁸ tetracysteine motif via thiol–arsenic exchange reactions that convert the nonfluorescent 1,2-ethanedithiol (EDT)-bound forms of these dyes into highly fluorescent protein-bound complexes. Despite their utility, however, biarsenicals are plagued by high background signals and cytotoxicity^{9,10} and can be challenging to apply in oxidizing cellular locales.^{11,12} Nontoxic, redox-insensitive alternatives that combine the convenience and selectivity of a biarsenical with the brightness of a fluorescent protein would be a valuable addition to the cell biologist’s “fluorescent toolbox”.² Here we report that [(3-oxospiro[isobenzofuran-1(3*H*),9′-[9*H*]xanthene]-3′,6′-diyl)bis(iminomethylene-2,1-phenylene)]bis-(9CI) (**RhoBo**, Figure 1A), a rhodamine-derived bisboronic acid described initially as a monosaccharide sensor,¹³ can function as a cell-permeable, turn-on fluorescent sensor for tetraserine motifs in engineered proteins.

It has been known since 1953 that phenyl boronic acid condenses with polyols to form boronate esters^{14,15} and since 1994 that the fluorescence of certain mono- and bis-boronic acid dyes increases upon esterification with simple sugars.^{16,17} The equilibrium stabilities of these complexes are low, however, with K_d values in the mM concentration range. We hypothesized that bis-boronic acid dyes would form higher affinity complexes with proteins containing a linear tetraserine motif. **RhoBo** was chosen as the ideal molecule with which to investigate this hypothesis, as it benefits from a simple synthesis and low monosaccharide affinity and forms boronate esters that emit at wavelengths > 500 nm,¹³ a useful range for experiments in live cells.

First, we asked whether **RhoBo** would form fluorescent complexes with peptides containing 2–4 serine residues separated by a variety of intervening sequences (Figures 1 and 2). Each peptide was incubated with **RhoBo** (17.1 μ M) in buffer at 37 °C, and the fluorescence emission at 580 nm was monitored as a function of peptide concentration. Under these conditions, peptide 1, containing the sequence Ser-Ser-Pro-Gly-Ser-Ser, formed the highest affinity complex with **RhoBo** ($K_{app} = 452 \pm 106$ nM). Titrations with peptides containing two serines rather than four (2) or shorter (3, 4) or longer (5) intervening sequences, or aspartate residues in place of serine (9), led to no detectable fluorescence change. Minimal fluorescence changes were observed with peptides containing threonine (7) or tyrosine (8) in place of serine. No fluorescence change was observed when **RhoBo** was incubated

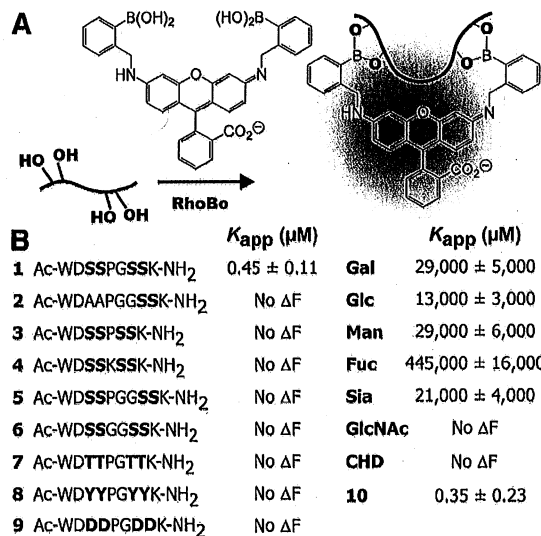


Figure 1. (A) Scheme illustrating a likely mode of condensation between **RhoBo** and a compound containing four hydroxyl groups. (B) Apparent equilibrium dissociation constant (K_{app}) of complexes between **RhoBo** and the peptides and monosaccharides shown.

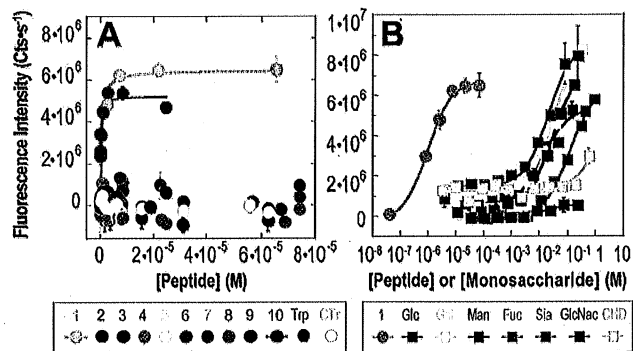


Figure 2. Changes in the fluorescence emission of **RhoBo** (17.1 μ M) in the presence of (A) peptides 1–10 and (B) indicated monosaccharides. Reactions were incubated in 100 mM phosphate buffer (pH 7.4) supplemented with 10% DMSO (37 °C, 60 min) and the emission monitored at 580 nm. Each point represents the average of three or more independent trials \pm the standard error.

with the serine proteases trypsin or chymotrypsin. Notably, the equilibrium stability and brightness of the **RhoBo**•1 complex (3955.5 $M^{-1} cm^{-1}$) compares favorably with the complex formed between ReAsH-EDT₂ and the optimized tetracysteine sequence FLNCCPGC-CMEP.¹⁸ **RhoBo** also formed a high affinity complex with a small well-folded protein, a derivative of the 36-aa pancreatic fold polypep-

[†] Department of Chemistry, Yale University.

[‡] Department of Molecular, Cellular, and Developmental Biology, Yale University.

[§] Department of Cell Biology, Yale University School of Medicine.

Catalytic Stamp Lithography for Sub-100 nm Patterning of Organic Monolayers

Hidenori Mizuno and Jillian M. Buriak*

Department of Chemistry, University of Alberta, and the National Institute for Nanotechnology (NINT), Edmonton, Alberta, Canada T6G 2G2

Received September 30, 2008; E-mail: jhuriak@ualberta.ca

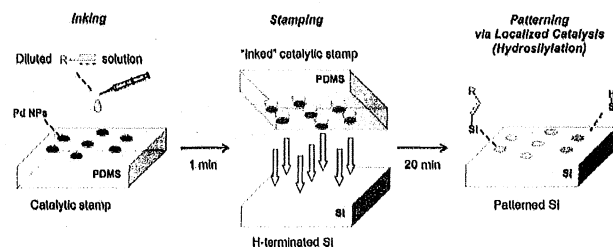
Patterning of organic nanostructures^{1–6} to control surface chemistries on technologically relevant substrates is of wide interest for the realization of molecular-scale engineering, ranging from electronics² to bioactive interfaces.³ In addition to the traditional photolithographic approach,⁴ imprint lithography-based techniques can provide a high throughput, large-area, and cost-effective route for this purpose.^{5a} Microcontact printing (μ CP), for example, has become a widely used, viable patterning tool to produce organic micron-scale motifs,^{5b} but challenging problems such as ink diffusion and stamp deformation make sub-100 nm patterning less routine.^{5a,c,d} Catalytic molecular transformations, as demonstrated by scanning probe techniques,⁶ are promising to this end, and its μ CP offshoot has just emerged recently.⁷ Herein, we describe our approach toward sub-100 nm patterning of organic monolayers through the integration of catalysis and stamping: catalytic stamp lithography.

Our strategy was initiated through the design of a novel type of patterning medium, a PDMS-based stamp patterned with an array of transition metal nanoparticle (NP) catalysts.⁸ Briefly, pseudo-hexagonal close packed NP arrays, presynthesized on oxide-capped silicon substrates via the use of self-assembled block copolymer (polystyrene-*block*-poly-2-vinylpyridine; PS-*b*-P2VP) templates,⁹ were transferred onto a surface of PDMS through a simple peel-off procedure (Supporting Information, SI). Due to the truncated cone shape of the NPs, the PDMS–NP interface is flat, leading to good contact with the printed surface (SI). Via modulation of the molecular weight of the PS and/or P2VP blocks, nanopatterns of various metals can be synthesized with center-to-center spacings of, for instance, 50–180 nm and nanoparticle diameters of 10–70 nm (Au, Ag, Pd, Pt; Si).⁹ A similar transfer approach was reported by Spatz et al. to fabricate patterned Au NPs on hydrogels for cell adhesion studies.¹⁰ The use of the self-assembly based process to produce catalytic stamps is inexpensive and efficient, since e-beam, nanoimprint lithography, and other techniques to produce the parent masters are avoided.

The demonstrative reaction employed here was Pd NP-catalyzed hydrosilylation¹¹ of terminal alkenes/alkynes on H-terminated Si surfaces. Because the reaction is catalyzed by solid NPs, pattern formation is not affected by ink diffusion or stamp deformation (localized catalysis). Direct chemical modification of Si substrates¹² is an ideal starting point for a broad range of applications. Scheme 1 illustrates the typical conditions of catalytic stamp lithography: a Pd catalytic stamp was inked with a dilute solution of terminal alkenes/alkynes for 1 min and then applied to freshly prepared flat H-terminated Si [either (100) or (111)]. Stamping was normally carried out for 20 min under light continuous pressure. The subsequent release of the catalytic stamp resulted in a duplication of the original pattern of Pd NPs on the silicon surface with arrays

of alkyl/alkenyl groups covalently attached to Si surface; the released stamp was reusable for subsequent inking/stamping (*vide infra*).

Scheme 1^a



^a Typical reaction conditions for catalytic stamp lithography (1 min inking and 20 min stamping) and the concept of localized catalysis. Catalytic hydrosilylation takes place only underneath Pd NPs.

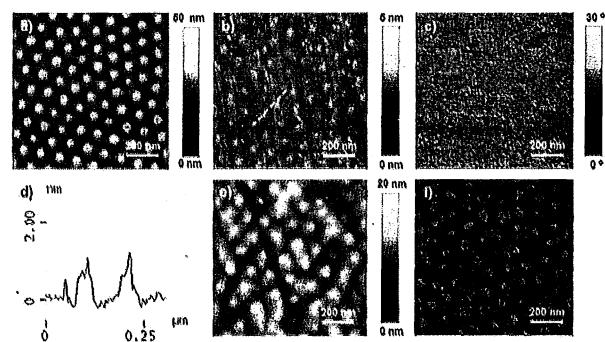


Figure 1. (a) AFM height image of a parent Pd catalytic stamp with NP diameters of 40 nm and a center-to-center spacing of 110 nm. (b) 1-Octadecyne-stamped Si(111)–H surface and corresponding phase image (c). (d) Section analysis along the dashed line in (b). (e) AFM height image of a 1-octadecyne-stamped Si(111)–H surface, followed by wet chemical etching with 40% NH_4F (aq). (f) SEM image of the sample from (e).

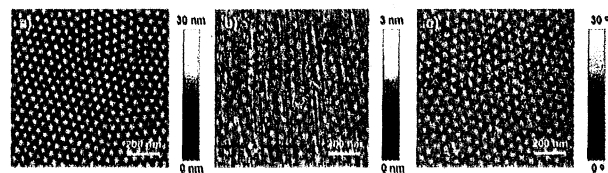


Figure 2. (a) AFM height image of a Pd catalytic stamp with NP diameters of 20 nm and center-to-center spacing of 60 nm. AFM height (b) and phase (c) images of the 5-hexyn-1-ol stamped Si(111)–H surface.

Figure 1 summarizes the results of catalytic stamp lithography (a–d) and its subsequent use as an etch stop (e,f), using a 5 mM 1,4-dioxane solution of 1-octadecyne as an ink. Tapping mode AFM height images of a Pd catalytic stamp and a stamped Si(111)–H

Evolution of Penicillin-Binding Protein 2 Concentration and Cell Shape during a Long-Term Experiment with *Escherichia coli*[∇]

Nadège Philippe,^{1,2,†} Ludovic Pelosi,^{1,2,†‡} Richard E. Lenski,³ and Dominique Schneider^{1,2,*}

Laboratoire Adaptation et Pathogénie des Micro-organismes, Université Joseph Fourier Grenoble 1, BP 170, F-38042 Grenoble cedex 9, France¹; CNRS UMR 5163, F-38042 Grenoble Cedex 9, France²; and Department of Microbiology and Molecular Genetics, Michigan State University, East Lansing, Michigan 48824³

Received 9 October 2008/Accepted 17 November 2008

Peptidoglycan is the major component of the bacterial cell wall and is involved in osmotic protection and in determining cell shape. Cell shape potentially influences many processes, including nutrient uptake as well as cell survival and growth. Peptidoglycan is a dynamic structure that changes during the growth cycle. Penicillin-binding proteins (PBPs) catalyze the final stages of peptidoglycan synthesis. Although PBPs are biochemically and physiologically well characterized, their broader effects, especially their effects on organismal fitness, are not well understood. In a long-term experiment, 12 populations of *Escherichia coli* having a common ancestor were allowed to evolve for more than 40,000 generations in a defined environment. We previously identified mutations in the *pbpA* operon in one-half of these populations; this operon encodes PBP2 and RodA proteins that are involved in cell wall elongation. In this study, we characterized the effects of two of these mutations on competitive fitness and other phenotypes. By constructing and performing competition experiments with strains that are isogenic except for the *pbpA* alleles, we showed that both mutations that evolved were beneficial in the environment used for the long-term experiment and that these mutations caused parallel phenotypic changes. In particular, they reduced the cellular concentration of PBP2, thereby generating spherical cells with an increased volume. In contrast to their fitness-enhancing effect in the environment where they evolved, both mutations decreased cellular resistance to osmotic stress. Moreover, one mutation reduced fitness during prolonged stationary phase. Therefore, alteration of the PBP2 concentration contributed to physiological trade-offs and ecological specialization during experimental evolution.

Bacteria in nature must survive multiple stresses and repeated shifts between feast and famine conditions. When *Escherichia coli* experiences nutritional deprivation, its growth rate decreases sharply and the cells become more spherical and resistant to various other environmental stresses (27). Many of the morphological and physiological changes that occur during entry into “stationary” phase are associated with the cell envelope, especially the cell wall.

Peptidoglycan is the major component of the bacterial cell wall, and it affects osmotic stability and cell shape (78). Many of the final steps of peptidoglycan synthesis are catalyzed in the periplasm by the penicillin-binding proteins (PBPs) (40, 82). These enzymes are named for their binding to β -lactam antibiotics that inhibit cell wall biosynthesis. Twelve PBPs have been identified so far in *E. coli*, and they are classified as high-molecular-weight (HMW) and low-molecular-weight (LMW) PBPs. The HMW PBPs assemble both the glycan chain and the peptide cross-links of peptidoglycan and are further divided into class A

PBPs (PBP1a, PBP1b, and PBP1c), which are bifunctional enzymes that perform both transglycosylation and transpeptidation functions, and class B PBPs (PBP2 and PBP3), which are monofunctional transpeptidases (24). The LMW PBPs (PBP4, PBP5, PBP6, PBP7, DacD, AmpC, and AmpH) are monofunctional, and they modify peptidoglycan by either carboxypeptidase or endopeptidase activities (53).

Numerous studies have investigated the physiological roles of PBPs by mutating either the PBP-encoding genes or by inactivating the corresponding proteins using specific β -lactam antibiotics. Although the class A HMW PBPs are peptidoglycan synthases, their physiological role is still unclear. Multiple *Bacillus subtilis* mutants are viable, although they have increased average cell lengths and reduced cell diameters (41, 53), whereas in *E. coli* the absence of two class A PBPs caused cell lysis (83). The two *E. coli* class B HMW PBPs, PBP2 and PBP3, are the only HMW PBPs that are essential for cell elongation and division, respectively. Loss of PBP2 results in cells that are spherical instead of rod shaped; PBP2 mutants are unable to grow and divide in rich media (18) unless compensatory mutations are present (75, 76). By contrast, PBP3 is involved in peptidoglycan synthesis during septation, and the absence of PBP3 causes cell filamentation (10, 65). The LMW PBPs have been shown to be involved in the control of cell shape, and severe shape abnormalities have been detected in mutants defective for several of these PBPs (44, 45, 53).

It is often necessary to inactivate several PBP-encoding genes to observe a clear phenotypic effect, which raises interesting questions about the biological significance of each individual PBP, such as whether single mutations may have more

* Corresponding author. Mailing address: Laboratoire Adaptation et Pathogénie des Microorganismes, Institut Jean Roget, CNRS UMR5163, Université Joseph Fourier, Campus Santé, Domaine de la Merci, BP170, 38042 Grenoble Cedex 9, France. Phone: (33) 4 76 63 74 90. Fax: (33) 4 76 63 74 97. E-mail: dominique.schneider@ujf-grenoble.fr.

† N.P. and L.P. contributed equally to this study.

‡ Present address: Laboratoire de Biochimie et Biophysique des Systèmes Intégrés (BBSI), Institut de Recherches en Technologies et Sciences du Vivant (iRTSV), UMR 5092 CNRS-CEA-Université Joseph Fourier (UJF), CEA-Grenoble, 17 Avenue des Martyrs, 38054 Grenoble Cedex 9, France.

[∇] Published ahead of print on 1 December 2008.

Advertisement

Applied Photophysics

For circular dichroism and stopped-flow spectroscopy

jb ONLINE

HOME HELP FEEDBACK SUBSCRIPTIONS ARCHIVE SEARCH TABLE OF CONTENTS

Institution: Harvard Libraries | Sign In via User Name/Password

Originally published In Press as doi:10.1074/jbc.M414050200 on February 10, 2005

J. Biol. Chem., Vol. 280, Issue 16, 15921-15927, April 22, 2005

Global Transcriptional Programs Reveal a Carbon Source Foraging Strategy by *Escherichia coli*^{*†‡}

Mingzhu Liu[†], Tim Durfee[‡], Julio E. Cabrera[§], Kai Zhao[¶], Ding J. Jin[§], and Frederick R. Blattner^{‡||}

From the [†]Department of Genetics and [¶]McArdle Laboratory for Cancer Research, University of Wisconsin, Madison, Wisconsin 53706 and the [§]Transcription Control Section, Gene Regulation and Chromosome Biology Laboratory, Center for Cancer Research, NCI at Frederick, National Institutes of Health, Frederick, Maryland 21702

By exploring global gene expression of *Escherichia coli* growing on six different carbon sources, we discovered a striking genome transcription pattern: as carbon substrate quality declines, cells systematically increase the number of genes expressed. Gene induction occurs in a hierarchical manner and includes many factors for uptake and metabolism of better but currently unavailable carbon sources. Concomitantly, cells also increase their motility. Thus, as the growth potential of the environment decreases, cells appear to devote progressively more energy on the mere possibility of improving conditions. This adaptation is not what would be predicated by classic regulatory models alone. We also observe an inverse correlation between gene activation and rRNA synthesis suggesting that reappportioning RNA polymerase (RNAP) contributes to the expanded genome activation. Significant differences in RNAP distribution *in vivo*, monitored using an RNAP-green fluorescent protein fusion, from energy-rich and energy-poor carbon source cultures support this hypothesis. Together, these findings represent the integration of both substrate-specific and global regulatory systems, and may be a bacterial approximation to metazoan risk-prone foraging behavior.

Received for publication, December 14, 2004, and in revised form, January 26, 2005.

* This work was supported by National Institutes of Health/NIGMS Grant GM35682-17S1 (to F. R. B.). Frederick R. Blattner has financial interest in NimbleGen Systems, Inc., DNASTAR, Inc. and Scarab Genomics, Inc. The costs of publication of this article were defrayed in part by the payment of page

QUICK SEARCH: [advanced]

Author: Keyword(s):
Go
Year: Vol: Page:

Advertisement



This Article

- ▶ [Full Text](#)
- ▶ [Full Text \(PDF\)](#)
- ▶ [Supplemental Data](#)
- ▶ [All Versions of this Article:](#)
280/16/15921 most recent
M414050200v1
- ▶ [Alert me when this article is cited](#)
- ▶ [Alert me if a correction is posted](#)
- ▶ [Citation Map](#)

Services

- ▶ [Email this article to a friend](#)
- ▶ [Similar articles in this journal](#)
- ▶ [Similar articles in PubMed](#)
- ▶ [Alert me to new issues of the journal](#)
- ▶ [Download to citation manager](#)
- ▶ [Request Permissions](#)

Citing Articles

- ▶ [Citing Articles via HighWire](#)
- ▶ [Citing Articles via Google Scholar](#)

Google Scholar

- ▶ [Articles by Liu, M.](#)
- ▶ [Articles by Blattner, F. R.](#)
- ▶ [Search for Related Content](#)

PubMed

- ▶ [PubMed Citation](#)
- ▶ [Articles by Liu, M.](#)
- ▶ [Articles by Blattner, F. R.](#)

Related Collections

- ▶ [Papers Of The Week](#)

Social Bookmarking



Advertisement

Get
Jazzed
to
Meet
in
New
Orleans

2009
ASBMB Annual
Meeting

Direct rapid prototyping of PDMS from a photomask film for micropatterning of biomolecules and cells†

Hyundoo Hwang,†^a Gyumin Kang,†^a Ju Hun Yeon,^a Yoonkey Nam^{*a} and Je-Kyun Park^{*ab}

Received 18th June 2008, Accepted 19th August 2008

First published as an Advance Article on the web 20th October 2008

DOI: 10.1039/b810341k

The soft lithographic technique is a collection of simple and cost-effective patterning techniques which applies an elastomeric stamp to transfer a nano/micro-scale pattern. Patterning biological materials using soft lithography provides procedurally simple control of the surface chemistry and the cell environments. However, conventional methods for generating microstructures on a substrate require expensive clean room facilities and skillful training. Here we report a simple and inexpensive clean-room free process using a conventional photomask film as a master to fabricate elastomeric stamps or microfluidic channels. This ultra rapid prototyping technique was applied to print FITC labeled poly-L-lysine with a 10 μm feature size on a glass substrate using soft lithographic processes, such as micro-contact printing and micromolding in capillaries, for patterning human hepatocellular carcinoma cells, human skin fibroblasts and hippocampal neurons from E-18 Sprague-Dawley rat. This novel technique using a photomask film as a master would be very useful 'hands-on' tool for the generation of micro-patterned chemical or biological assays using cells and proteins.

Introduction

Micropatterning of biological materials such as proteins and cells is a powerful technique for several applications in biology and chemistry. The ability to pattern proteins at desired locations on a substrate is essential in a number of emerging technologies, including biosensors and biochips for biochemical analysis and diagnosis.¹ In addition, the patterning of cells is also necessary, especially in cell biology, not only for studying intercellular interactions,² cell shape changes,³ apoptosis⁴ and differentiation,⁵ but also for creating cell-based biosensors⁶ and microarrays.⁷

Although several patterning techniques such as photochemical methods,^{1,8} electrokinetic methods⁹ and direct spraying¹⁰ or spotting^{11,12} have been reported, soft lithographic methods, including micro-contact printing (μCP) and micromolding in capillaries (MIMIC), have attracted much attentions as one of the most simple, cost-effective, and convenient methods for patterning biological materials on a substrate.¹³ Soft lithographic techniques use an elastomeric stamp or mold to transfer a nano-/micro-scale pattern.¹⁴ Patterning proteins and cells using soft lithography provides procedurally simple control of the surface chemistry and the cell environments.^{13,15} However, conventional methods such as photolithography and electron beam lithography for generating microstructures on a silicon wafer require expensive clean-room facilities and skillful technicians, which are

usually not available for the real potential user group in biology and chemistry community.

For the simple rapid fabrication of microstructures, direct printing methods using an office laser printer have been reported.^{16–19} Bao *et al.* have directly utilized the laser-printed film as a master for a poly(dimethylsiloxane) (PDMS) microchannel which has applied for capillary electrophoresis.¹⁷ However, the laser-printed master, which was constructed with laser-printed toners on a polyester film, had too rough surface and low resolution (the minimum line width $\geq 100 \mu\text{m}$) to apply for other biological and chemical applications. Very recently, a toner was directly printed onto the copper sheet as a mask for the simple fabrication of master by selective wet-etching.¹⁹ However, the minimum feature size by this technique was still in the order of hundreds of micrometers as well as the etching processes are certainly required.

In this report, we demonstrate a simple, inexpensive, and clean-room free process to fabricate elastomeric stamps and molds, which have both smooth surface and high resolution, for soft lithographic micropatterning of biomaterials. A commercially available high-resolution photomask film was directly used as a master to produce PDMS stamps or microfluidic channels, and micrometer-scale cell patterns, including human hepatocellular carcinoma cells, human skin fibroblasts and hippocampal neurons from E-18 Sprague-Dawley rat, were created by patterning a cell-adhesive biomolecule, FITC-labeled poly-L-lysine (PLL-FITC) on a glass substrate with μCP and MIMIC.

Experimental

The desired micropatterns—spots, lines, and grids—were generated using a conventional computer-aided design (CAD) program and printed on a photomask film (0.25 mm-thickness; Kodak Co., Ltd., NY) using a conventional laser film printer (Laser

^aDepartment of Bio and Brain Engineering, KAIST, 335 Gwahangno, Yuseong-gu, Daejeon, 305-701, Korea. E-mail: jekyun@kaist.ac.kr; ynam@kaist.ac.kr; Fax: +82-42-350-4310; Tel: +82-42-350-4315; +82-42-350-4322

^bDepartment of Biological Sciences, KAIST, 335 Gwahangno, Yuseong-gu, Daejeon, 305-701, Korea

† Electronic supplementary information (ESI) available: Cell culture method. See DOI: 10.1039/b810341k

‡ These authors contributed equally to this work.

A microfluidic abacus channel for controlling the addition of droplets†

Eujin Um^a and Je-Kyun Park^{*ab}

Received 27th August 2008, Accepted 17th October 2008

First published as an Advance Article on the web 14th November 2008

DOI: 10.1039/b814948h

This paper reports the first use of the abacus-groove structure to handle droplets in a wide microchannel, with no external forces integrated to the system other than the pumps. Microfluidic abacus channels are demonstrated for the sequential addition of droplets at the desired location. A control channel which is analogous to biasing in electronics can also be used to precisely determine the number of added droplets, when all other experimental conditions are fixed including the size of the droplets and the frequency of droplet-generation. The device allows programmable and autonomous operations of complex two-phase microfluidics as well as new applications for the method of analysis and computations in lab-on-a-chip devices.

Introduction

At present, microfluidics comprises the essential part of lab-on-a-chip techniques as a means to transport experimental reagents or operate the working devices as a pump or valves.^{1,2} More recently, the field has extended to how the movement of fluids can convey information on a chip. Lab-on-a-chips can seek alternate solutions for data processing and representation by utilizing innate nonlinear characteristics of fluid dynamics on the micro-scale. Fluids themselves can generate dynamic signals in waveforms with microfluidic valves and mixing networks,³ or function as a bistable flip-flop memory using the viscoelastic property of the polymer solution.⁴ Laminar flow can perform the logical operation by making a selection of the path as a consequence of the flow resistance,⁵ and surface tension-driven pumping of droplets in the air through the microchannel can also be designed as logic gates and timers.⁶

Generating, controlling, and manipulating fluids in two-phase bubble or droplet forms has also found applications in microfluidic environments as microchambers of biological and chemical reaction for their abilities of compartmentalization, rapid mixing, and delivery of materials with precise control of reaction time.⁷⁻⁹ Moreover, the discrete nature of bubbles or liquid droplets in immiscible fluids is especially compatible to perform computational operations with each droplet representing a unit of information in a microfluidic circuit. Possibilities are found in the study of periodicity of bubble-oscillatory patterns in microfluidics,¹⁰ and reversibility of initial inter-droplet time intervals which can encode and decode signals and represent them as the binary number.¹¹ Path selection of droplets or bubbles in microchannels under the influence of flow resistance and the presence of other bubbles or droplets is also used to perform various logical operations.^{12,13} More studies on the behaviors of droplets which

“think”¹⁴ in the act of flowing will simplify the integration process of valves and switches usually required in fluid-based experiments.

Other characteristics of droplets that show potential in the field of fluidic computation include the ability of a droplet to merge with other droplets to form bigger ones or to split into smaller droplets. Also, the fact that velocity of the dispersed phase can be set to be different with the continuous phase flow carrying them can be the building block of a more complex circuit. Although splitting of a droplet is relatively easy with modification of the channel geometry that deforms and extends the shape of a sphere,¹⁵ merging of droplets is hard to achieve because both the time and the space have to be manipulated for synchronization of approaching droplets. If droplets have different sizes, they flow at different velocities in one channel and are able to merge in the downstream.¹⁶ Creating a velocity gradient using a tapered chamber allows droplet approaching by slowing down the flow rate and a slight increase in the distance between adjacent droplets when leaving the chamber facilitates the event of merging.^{17,18} A fluid rectifying channel also removes the continuous phase between droplets and allows merging of multiple droplets.¹⁹ Electric forces,^{20,21} or optical forces have been implemented to enhance the merge rate.²² However, previous results have been insufficient to quantitatively estimate the merging ratio of droplet numbers. When merging is accomplished by changing the flow rates of the continuous phase or dispersed phase, other factors such as the size of droplets or the pattern of droplet-generating states are immediately affected.^{19,23,24} Also, the location of droplet merging in the channel is hard to predict in the stream of continuous flow. The systems have to overcome the limited range of flow rates and the size of droplets on the events of droplet addition. Temporal trapping or retention of a droplet in a designated place will be suitable for efficient merging and temporal storage of information in a microfluidic circuit, although permanent storage of droplets has been accomplished with surface tension-guided docking sites.²⁵

In this work, we have integrated the functions of temporal stopping, merging, and splitting of droplets into one device to design a controllable droplet adder. The microchannel structure mimics an ancient counting tool, abacus, still used in Asian countries today. The method of counting is very intuitive. Counting beads slide in grooves or along wires one by one. Our device adopts the approach of assembling liquid droplets in the

^aDepartment of Bio and Brain Engineering, KAIST, 335 Gwahangno, Yuseong-gu, Daejeon, 305-701, Korea. E-mail: jekyun@kaist.ac.kr; Fax: +82-42-350-4310; Tel: +82-42-350-4315

^bDepartment of Biological Sciences, KAIST, 335 Gwahangno, Yuseong-gu, Daejeon, 305-701, Korea

† Electronic supplementary information (ESI) available: Video clip 1–3 for droplet addition in a microchannel. See DOI: 10.1039/b814948h

Integrated two-step gene synthesis in a microfluidic device†

Mo Chao Huang, Hongye Ye, Yoke Kong Kuan, Mo-Huang Li* and Jackie Y. Ying

Received 6th May 2008, Accepted 19th August 2008

First published as an Advance Article on the web 23rd October 2008

DOI: 10.1039/b807688j

Herein we present an integrated microfluidic device capable of performing two-step gene synthesis to assemble a pool of oligonucleotides into genes with the desired coding sequence. The device comprised of two polymerase chain reactions (PCRs), temperature-controlled hydrogel valves, electromagnetic micromixer, shuttle micromixer, volume meters, and magnetic beads based solid-phase PCR purification, fabricated using a fast prototyping method without lithography process. The fabricated device is combined with a miniaturized thermal cycler to perform gene synthesis. Oligonucleotides were first assembled into genes by polymerase chain assembly (PCA), and the full-length gene was amplified by a second PCR. The synthesized gene was further separated from the PCR reaction mixture by the solid-phase PCR purification. We have successfully used this device to synthesize a green fluorescent protein fragment (GFPuv) (760 bp), and obtained comparable synthesis yield and error rate with experiments conducted in a PCR tube within a commercial thermal cycler. The resulting error rate determined by DNA sequencing was 1 per 250 bp. To our knowledge, this is the first microfluidic device demonstrating integrated two-step gene synthesis.

Introduction

The design and manufacture of custom genes or long DNA biomolecules is fast becoming an indispensable tool in synthetic biology¹ and protein engineering.^{2,3} The DNA biomolecules with man-made sequences are constructed by assembling pools of oligonucleotides into larger DNA using *de novo* synthesis methods. As the DNA structures can be custom designed and chemically synthesized, this technology has enabled broad applications on the engineering of proteins with novel functions,⁴ artificial gene networks,⁵ and synthetic genomes.^{6–8}

Researchers have successfully utilized the *de novo* gene synthesis methods to assemble a viral genome⁶ (7.5 kb) in 2002, bacteriophage genome⁷ (5.4 kb) in 2003, and a gene cluster⁹ as large as 32 kb in 2004. The longest synthetic DNA reported to date is 582 kb, the genome of a bacterium (*Mycoplasma genitalium*) by Venter and co-workers⁸ in 2008. Furthermore, DNA synthesis has been successfully combined with high-density DNA microarray technologies,^{10,11} providing millions of unique oligonucleotides at a significantly lower cost (on the order of 1 cent per oligonucleotide) compared to the conventionally synthesized oligonucleotides (USD 0.2 per base). DNA biomolecules as large as 15 kb¹⁰ has been successfully constructed with oligonucleotides from a DNA microarray thus far.

The most reported method for constructing long DNA was based on the PCR process, which relied on the use of overlapped oligonucleotides to construct genes. Various PCR-based methods have been proposed in an attempt to optimize the PCR process for long DNA sequences and to enhance the accuracy of assembly. These methods are the thermodynamically balanced inside-out (TBIO) method,¹² successive PCR,¹³ dual

asymmetrical PCR (DA-PCR),¹⁴ overlap extension PCR (OE-PCR)^{15,16} and PCR-based two-step DNA synthesis (PTDS).¹³ Fig. 1 shows the concept of the two-step overlapping gene assembly method¹⁵ to create a synthetic gene. A pool of short oligonucleotides is first assembled into long double-stranded DNA (called a template) with the desired length and sequence information using the polymerase cycling assembly (PCA).¹⁷ The quantity of the assembled template DNA is then amplified by the PCR step. The PCR assembly utilizes the DNA polymerase to extend the oligonucleotides. As the mixed oligonucleotide is subjected to PCR, the overlap at their 3' ends are extended to generate longer double-stranded products. This process is repeated for the double-stranded products until the full-length gene is obtained. Synthesis *via* PCR can be performed either as a one-step process, combining assembly PCR and amplification PCR into a single stage, or as a two-step process with separate stages for assembly and amplification.

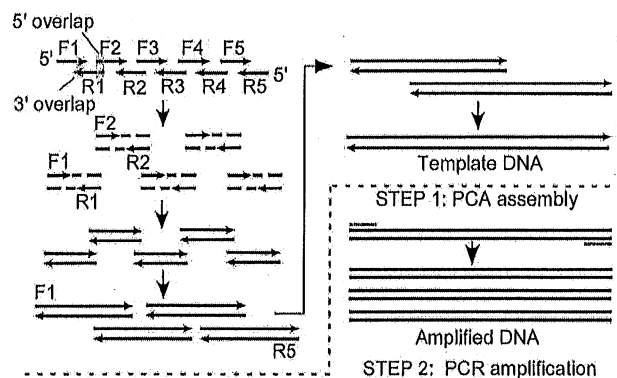


Fig. 1 Schematic illustration of PCR-based gene synthesis. One-step synthesis combines PCA and PCR amplification into a single stage. The two-step synthesis is performed with separate stages for assembly and amplification.

Institute of Bioengineering and Nanotechnology, 31 Biopolis Way, The Nanos, Singapore 138669. E-mail: mhl1@ibn.a-star.edu.sg

† Electronic supplementary information (ESI) available: Table S1. See DOI: 10.1039/b807688j

In-situ measurement of cellular microenvironments in a microfluidic device

Zhang Lin, Tan Cherng-Wen, Partha Roy and Dieter Trau*

Received 23rd April 2008, Accepted 19th August 2008

First published as an Advance Article on the web 23rd October 2008

DOI: 10.1039/b806907g

We report on the integration of optical microsensors into a cell culture microchannel device. We demonstrate the possibility of measuring the glucose and oxygen concentrations in the microenvironment of the mammalian cells cultured in a microchannel device. Furthermore, cell proliferation and morphology could be monitored microscopically while these measurements were being made. Through the use of multiple sensors along the length of the microchannel, concentration gradients of various metabolites, such as oxygen, as well as the effects of cell uptake and perfusion rate of growth medium on these gradients could be studied. As such, the system allowed real-time observations of the cells' response to their chemical microenvironment. Our approach allows cell culture and cell assays to be performed simultaneously in an integrated microchannel system with potential applications as a research tool or drug screening method.

Introduction

Since its emergence, microfluidics has been revolutionizing many research areas including molecular biology, cell biology, environmental analysis and medical diagnosis.¹⁻³ One key application of microfluidics is to culture cells in microfluidic devices, challenging the conventional Petri dish and culture flask-based cell culture methodology. Microfluidics-based cell culture systems can provide a level of control over the cell culture microenvironment that cannot be achieved under traditional culture conditions. Microfluidics can reproducibly produce confined and well-defined systems such as microchannels on the cellular length scale (5 μm - 500 μm), incorporate complex designed topographies, establish various densities of extracellular matrix signaling molecules, and offers the unique ability to mimic in-vivo solution flow.⁴ To date, many microfluidic systems have been built for culturing different cell lines, and their strong capabilities in simulating in-vivo cell growth and development, as well as providing greater control both temporally and spatially over the cell culture microenvironment have been successfully demonstrated.⁵⁻¹²

However, analysis of the cellular microenvironment in microfluidic platforms remains an issue to be addressed. The difficulty here is largely due to the fundamental differences between the cellular microenvironment under microfluidic conditions and those under traditional cell culture conditions.¹³ In macroscale cell culture, large volumes of medium are readily available to ensure the cultured cells have access to necessary metabolites; convection by stirring or shaking generates homogenous distribution of metabolites within the entire cell culture medium with minimized waste accumulation. In the microscale, diffusion becomes the dominant force and laminar flow makes mixing very difficult. This results in a less homogeneous distribution of metabolites and waste products, which in

turn leads to the failure of those detection methods developed for conventional macroscale systems. Besides, the relatively small volume of the sample manipulated in microfluidics makes any centrifuge tube or microplate-based assay literally impossible.

In an attempt to solve these problems, we designed and developed a hybrid microfluidic system enabling cell culture with on-chip microenvironment sensing capabilities. This integrated approach allows in-situ measurement of the cellular microenvironment, and it doesn't require the addition of any reagents or transfer of the sample elsewhere. In other words, the new method allows us to maintain the microenvironment intact throughout the measurement process and provides us with real-time information about the chemical and biological parameters of interest.

This was achieved by merging different technologies including microfabrication, fluorescence optical sensing and advanced biomaterial encapsulation techniques. A modified photolithography method was developed to fabricate a double-layered microfluidic device, with the microchannel layer intended for cell culture and the microtrench layer for immobilization of sensing biomaterials. Fluorescence-based optical sensing was the sensor of choice, given its high sensitivity and ease of integration with the device. A matrix-assisted layer-by-layer (LbL) coating technique was used for encapsulation of the sensors.¹⁴ β -TC-6 (a transgenic insulin-secreting cell line derived from mice) was cultured in the microfluidic device, and in-situ measurement of glucose and oxygen concentrations in the cellular microenvironment was demonstrated.

Experimental methods

Chip design

A diagram of the chip is shown in Fig. 1A. The chip features a double-layered design: one layer comprising the microchannel in which the cells would be cultured and another layer of microtrenches for the immobilization of the sensing materials. Each microtrench is an indentation on the surface of the microchannel (enlarged in inset of Fig. 1A). Seven microtrenches, each

Division of Bioengineering, National University of Singapore, Singapore.
E-mail: bietrau@nus.edu.sg; Fax: (65) 65163069

Petri dish PCR: laser-heated reactions in nanoliter droplet arrays

Hanyoung Kim, Siarhei Vishniakou and Gregory W. Faris*

SRI International, 333 Ravenswood Avenue, Menlo Park, CA, USA. E-mail: gregory.faris@sri.com; Fax: +1 650 859 6196; Tel: +1 650-859-4131

Received 3rd October 2008, Accepted 12th December 2008

First published on the web 19th January 2009

We report high-speed real-time PCR performed on an unmodified disposable polystyrene Petri dish. The reaction cycle relies solely on an infrared laser for heating; no conventional heater is required. Nanoliter droplets of PCR mixture as water-in-oil emulsions printed in an array format served as individual PCR microreactors. A simple contact printing technique was developed to generate a large array of uniform sized nanoliter droplets using disposable pipette tips. Printed droplets showed variation of less than 10% in volume and the oil/water/polystyrene interface formed a compact droplet microreactor approximately spherical in shape. The uniform droplet array was used to optimize the laser power required for the two heating steps of PCR, annealing/extension and melting, while the ambient conditions were at room temperature. The optical heating allows for an extremely fast heating rate due to the selective absorption of the infrared laser by PCR buffer only and not the oil or polystyrene Petri dish, allowing completion of 40 amplification cycles in ~6 minutes. The quantitative assay capability of the system is also presented and discussed.

Introduction

Aqueous solutions dispersed in an oil phase (inverted emulsions) have been widely tested and adopted as ideal microreactors especially for high-throughput lab-on-a-chip applications.¹⁻³ Successful executions of many biochemical reactions have been demonstrated in a single droplet without affecting neighboring droplets⁴⁻⁸ including polymerase chain reaction (PCR) in nano to picoliter volume droplets.⁹⁻¹⁴ This broad use of droplet methods covering a range of applications is due to the droplet's high stability, low volume required per droplet, absence of cross talk between droplets when separated by the oil phase, and the straightforward production of a large number of reaction wells or droplets without any microfluidic device.¹⁵ Moreover, recently developed techniques for manipulation of individual droplets on a planar substrate, microfluidics without channels,^{9,16,17} set the stage for the direct application of droplet-based methods to highly parallel assays with microfluidic control methods that can also perform the sample preparation steps such as heating and mixing. Such a high-throughput system naturally requires a suitable droplet generation in a controlled manner. Various channel- or chip-based systems have been developed to meet this requirement.^{6,17-20} However, the microfabrication of microfluidic and/or electrical circuitry on the substrate is often time consuming and expensive. Furthermore, any reuse of a microfluidic substrate runs the risk of cross contamination between samples. For this work on PCR in nanoliter droplets, we prepare droplet arrays using contact printing²¹ as shown in Fig. 1 (a).

Robust and sensitive control of a quorum-sensing circuit by two interlocked feedback loops

Joshua W Williams¹, Xiaohui Cui¹, Andre Levchenko^{2,*} and Ann M Stevens^{1,*}

¹ Department of Biological Sciences, Virginia Tech, Blacksburg, VA, USA and ² Department of Biomedical Engineering, Johns Hopkins University, Baltimore, MD, USA
* Corresponding authors. A Levchenko, Department of Biomedical Engineering, Johns Hopkins University, 208C Clark Hall, 3400 N Charles Street, Baltimore, MD 21218, USA. Tel.: +1 410 516 5584; Fax: +1 410 516 4771; E-mail: alev@jhu.edu or AM Stevens, Department of Biological Sciences, Virginia Tech, 219 Life Sciences 1 (0910), Washington Street, Blacksburg, VA 24061, USA. Tel.: +1 540 231 9378; Fax: +1 540 231 4043; E-mail: ams@vt.edu

Received 12.3.08; accepted 24.10.08

The quorum-sensing (QS) response of *Vibrio fischeri* involves a rapid switch between low and high induction states of the *lux* operon over a narrow concentration range of the autoinducer (AI) 3-oxo-hexanoyl-L-homoserine lactone. In this system, LuxR is an AI-dependent positive regulator of the *lux* operon, which encodes the AI synthase. This creates a positive feedback loop common in many bacterial species that exhibit QS-controlled gene expression. Applying a combination of modeling and experimental analyses, we provide evidence for a LuxR autoregulatory feedback loop that allows LuxR to increase its concentration in the cell during the switch to full *lux* activation. Using synthetic *lux* gene fragments, with or without the AI synthase gene, we show that the buildup of LuxR provides more sensitivity to increasing AI, and promotes the induction process. Elevated LuxR levels buffer against spurious variations in AI levels ensuring a robust response that endows the system with enhanced hysteresis. LuxR autoregulation also allows for two distinct responses within the same cell population.

Molecular Systems Biology 16 December 2008; doi:10.1038/msb.2008.70

Subject Categories: simulation and data analysis; signal transduction

Keywords: bistability; hysteresis; *lux* operon; quorum sensing; *Vibrio fischeri*

This is an open-access article distributed under the terms of the Creative Commons Attribution Licence, which permits distribution and reproduction in any medium, provided the original author and source are credited. Creation of derivative works is permitted but the resulting work may be distributed only under the same or similar licence to this one. This licence does not permit commercial exploitation without specific permission.

Introduction

Quorum sensing (QS) is an example of cell–cell communication in bacteria, allowing an assemblage of closely positioned cells to alter its behavior in a coordinated manner, if the cell density exceeds a specific threshold. QS regulates a plethora of critically important phenotypes, including antibiotic production, release of exoenzymes, production of virulence factors, induction of genetic competency, conjugative plasmid transfer, biofilm formation and bioluminescence (Fuqua *et al.*, 2001; Waters and Bassler, 2005; Reading and Sperandio, 2006). In addition to understanding the role of these bacterial phenotypes to pathogenic and symbiotic states, analysis of the mechanisms underlying QS might shed light on how the behavior of a single cell can be tightly and robustly coordinated with the behavior of the cell group.

The QS response of *Vibrio fischeri* is a model system for many other QS systems that share networks similar to the LuxR/I network (Taga and Bassler, 2003). LuxR is an autoinducer (AI)-dependent positive regulator of the *lux* operon, and LuxI produces the AI molecule, 3-oxo-hexanoyl-L-homoserine lactone. Much is known about how the LuxR/I system achieves activation of the *lux* operon leading to

bioluminescence. A number of factors, including the activator complex cAMP–CRP, regulate the expression of *luxR* (Friedrich and Greenberg, 1983; Dunlap and Greenberg, 1985, 1988). LuxR then activates expression of the *lux* operon when the concentration of LuxR–AI complexes reaches a critical threshold. This leads to higher levels of AI, generating a positive feedback loop (Dunlap and Greenberg, 1988; Choi and Greenberg, 1992; Stevens and Greenberg, 1999; Lupp *et al.*, 2003). It has been proposed that LuxR not only regulates the *lux* operon but it might also positively or negatively autoregulate the QS response through modulating its own expression (Dunlap and Ray, 1989; Shadel and Baldwin, 1991, 1992; Chatterjee *et al.*, 1996), although the precise molecular basis for this autoregulation remains unknown.

The presence of one or more feedback interactions in the molecular networks underlying QS in *V. fischeri* and other bacterial systems might lead to such emergent properties as hysteretic responses and the associated ‘memory’ of the previous network states. Such memory-like properties have been suggested for other systems containing positive feedback interactions, based both on mathematical modeling and experimental investigation (Ferrell, 2002; Levchenko, 2003; Sha *et al.*, 2003; ; Angeli *et al.*, 2004; Ninfa and Mayo, 2004;

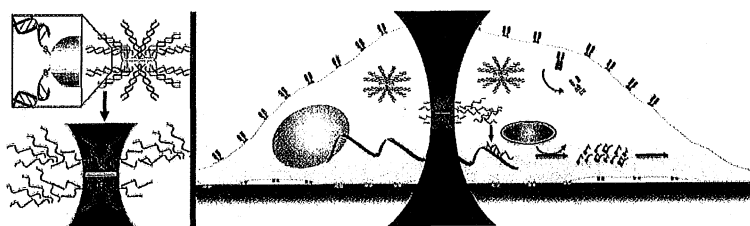
Letter

Remote Optical Switch for Localized and Selective Control of Gene Interference

Somin Eunice Lee, Gang Logan Liu, Franklin Kim, and Luke P. Lee

Nano Lett., Article ASAP • DOI: 10.1021/nl802689k

Downloaded from <http://pubs.acs.org> on January 22, 2009



More About This Article

Additional resources and features associated with this article are available within the HTML version:

- Supporting Information
- Access to high resolution figures
- Links to articles and content related to this article
- Copyright permission to reproduce figures and/or text from this article

[View the Full Text HTML](#)



ACS Publications
High quality. High impact.

Nano Letters is published by the American Chemical Society, 1155 Sixteenth Street N.W., Washington, DC 20036

LETTERS

A tunable synthetic mammalian oscillator

Marcel Tigges¹, Tatiana T. Marquez-Lago^{1,2,3}, Jörg Stelling^{1,2,3} & Martin Fussenegger¹

Autonomous and self-sustained oscillator circuits mediating the periodic induction of specific target genes are minimal genetic time-keeping devices found in the central and peripheral circadian clocks^{1,2}. They have attracted significant attention because of their intriguing dynamics and their importance in controlling critical repair³, metabolic⁴ and signalling pathways⁵. The precise molecular mechanism and expression dynamics of this mammalian circadian clock are still not fully understood. Here we describe a synthetic mammalian oscillator based on an auto-regulated sense-antisense transcription control circuit encoding a positive and a time-delayed negative feedback loop, enabling autonomous, self-sustained and tunable oscillatory gene expression. After detailed systems design with experimental analyses and mathematical modelling, we monitored oscillating concentrations of green fluorescent protein with tunable frequency and amplitude by time-lapse microscopy in real time in individual Chinese hamster ovary cells. The synthetic mammalian clock may provide an insight into the dynamics of natural periodic processes and foster advances in the design of prosthetic networks in future gene and cell therapies.

Synthetic gene circuits that emulate the expression dynamics of living systems provide new insights into the connectivity of genes and proteins in the postgenomic era⁶ and they advance our understanding of complex control networks. Circadian pacemakers^{7,8} are of particular interest because they coordinate many periodic physiological activities. The mammalian circadian clock consists of a central pacemaker in the suprachiasmatic nuclei of mammalian brains⁹, with subsidiary oscillators in most peripheral cell types^{4,5,10}. In contrast to neurons in the suprachiasmatic nuclei, peripheral oscillators damp rapidly when disconnected from remote control by the suprachiasmatic nuclei¹⁰. However, both oscillators rely on a very similar gene circuitry that involves a set of transcriptional repressors (CRY and PER) and activators (BMAL1 and CLOCK) connected by mutual feedback¹¹. Previously designed simple synthetic gene networks in bacteria showed self-sustained¹², damped¹³ or metabolically controlled oscillations¹⁴, but those oscillators lacked robustness and/or tunability. In mammalian cells, even synthetic clock replicas using natural components and network design have not provided oscillating transgene expression¹⁵ as observed for reporter genes plugged

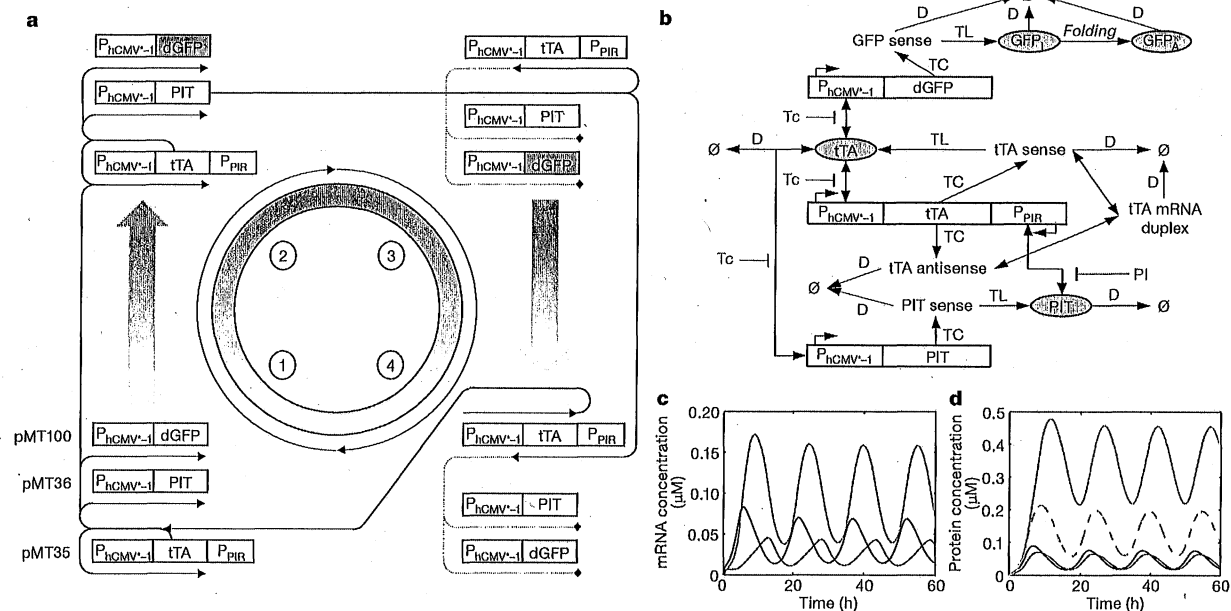


Figure 1 | Mammalian clock components and predicted oscillation dynamics. **a**, Core mammalian oscillator. Autoregulated $P_{hCMV^{*1}}$ -driven tTA transcription triggers increasing expression of sense tTA (pMT35), Ub^{V76}-GFP (pMT100) and PIT (pMT36) (1). As Ub^{V76}-GFP and PIT levels reach a peak (2), PIT steadily induces P_{PIR} -driven tTA anti-sense expression (3), resulting in a gradual decrease in sense tTA, PIT and Ub^{V76}-GFP (4). **b**, Intracellular processes considered in the mathematical model. Abbreviations and symbols are as follows: single-headed arrows, irreversible

reactions; double-headed arrows, reversible reactions; \emptyset , sinks for degradation processes; dGFP, destabilized GFP; Tc, tetracycline; PI, pristinamycin I; GFP_I, unfolded inactive GFP; GFP_A, folded active GFP; TC, transcription; TL, translation; D, degradation. **c**, **d**, Model predictions for the reference parameter set (plasmid ratios 1:1:1, no antibiotics) with mRNA concentrations (c) (black, tTA; blue, PIT; red, tTA-sense-antisense duplex) and protein concentrations (d) (black, tTA; blue, PIT; dashed green, unfolded GFP; solid green, active GFP).

¹Department of Biosystems Science and Engineering, ETH Zurich, Mattenstrasse 26, CH-4058 Basel, Switzerland. ²Institute of Computational Science and ³Swiss Institute of Bioinformatics, ETH Zurich, CH-8092 Zurich, Switzerland.

Quality control by the ribosome following peptide bond formation

Hani S. Zaher¹ & Rachel Green¹

The overall fidelity of protein synthesis has been thought to rely on the combined accuracy of two basic processes: the aminoacylation of transfer RNAs with their cognate amino acid by the aminoacyl-tRNA synthetases, and the selection of cognate aminoacyl-tRNAs by the ribosome in cooperation with the GTPase elongation factor EF-Tu. These two processes, which together ensure the specific acceptance of a correctly charged cognate tRNA into the aminoacyl (A) site, operate before peptide bond formation. Here we report the identification of an additional mechanism that contributes to high fidelity protein synthesis after peptidyl transfer, using a well-defined *in vitro* bacterial translation system. In this retrospective quality control step, the incorporation of an amino acid from a non-cognate tRNA into the growing polypeptide chain leads to a general loss of specificity in the A site of the ribosome, and thus to a propagation of errors that results in abortive termination of protein synthesis.

The overall *in vivo* rate of misincorporation during protein synthesis has been estimated to be in the range of 6×10^{-4} to 5×10^{-3} per amino acid incorporated^{1,2}. Current models for the mechanisms governing this level of accuracy focus on the accurate charging of tRNAs with their cognate amino acid by the aminoacyl-tRNA synthetases and correct tRNA selection by the ribosome facilitated by the GTPase elongation factor EF-Tu in bacteria (or eEF1A in eukaryotes). Kinetic discrimination mechanisms, driven by induced fit, have been demonstrated for the synthetases and the ribosome to facilitate accurate selection of amino acids or charged tRNAs, respectively^{3,4}. In addition, for both processes, proofreading (or editing) mechanisms have been shown to increase the overall fidelity further^{3,5-7}. Experimental measurements of *in vitro* aminoacylation accuracy ($\sim 10^5$) agree well with that observed *in vivo*⁸. *In vitro* protein synthesis systems (generally poly-Phe synthesis on polyU) have been shown to proceed with an overall fidelity (combining the tRNA selection and proofreading steps) of as high as 10^{-4} (refs 3, 9 and 10). However, fidelity measurements in our own laboratory conducted in the full range of published buffer systems with tRNA mixtures on heteropolymeric messenger RNA suggest that *in vitro* protein synthesis proceeds with slower fidelity (an error rate of 2×10^{-3} to 10×10^{-3} ; Supplementary Fig. 1), thus arguing that further quality control mechanisms may exist.

Here we identify a previously uncharacterized ribosome-centred mechanism that contributes to translational quality control, and which may help explain discrepancies between *in vitro* and *in vivo* measured fidelity values. The surprising feature of this pathway is that it monitors the fidelity of protein synthesis after the formation of a peptide bond (retrospectively), in certain ways analogous to the exonucleolytic proofreading step in DNA replication¹¹. We provide evidence that the ribosome recognizes errors during synthesis by evaluating the codon-anticodon helix in the peptidyl (P) site of the small subunit of the ribosome, leading first to reduced fidelity during subsequent tRNA selection and ultimately to premature termination by release factors.

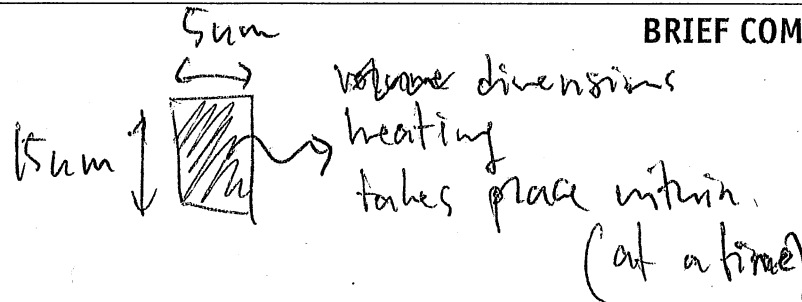
A mismatched P site triggers unusual release behaviour

During the course of reconstituting *in vitro* the translation of ribosome nascent chain complexes (RNCs), with the core elongation

steps shown in Fig. 1a, we identified an abundant miscoding event in which Lys-tRNA^{Lys} (anticodon UUU) efficiently decoded an AAU Asn codon in a short peptide sequence, as previously documented *in vivo*¹². In these reactions, we observed that in miscoded ribosome complexes the peptidyl-tRNA did not efficiently react to incorporate the next amino acid encoded by the mRNA, but instead seemed to be promiscuously hydrolysed. These data suggested the existence of a quality control step that follows peptide bond formation and effectively functions to terminate translation of aberrant protein products, thus enhancing the overall fidelity of protein synthesis.

To characterize this unusual observation, we produced RNCs carrying a dipeptidyl-tRNA in the P site with either a matched or a mismatched codon-anticodon helix and a variety of different codons in the A site. We started with a pair of RNCs containing a stop codon in the A site (mRNAs encoding MKX (AUG AAA UGA) or MNX (AUG AAU UGA)) to check anticipated release factor 2 (RF2) properties on these complexes. Complexes were assembled in a simplified reaction mixture containing initiation factors (IF1-IF3) and fMet-tRNA^{fMet}, and were reacted with ternary complex (Lys-tRNA^{Lys}-EF-Tu-GTP) in the presence of elongation factor EF-G to yield ribosome complexes with fMet-Lys-tRNA^{Lys} in the P site (Fig. 1b and Supplementary Fig. 2), followed by purification over a sucrose cushion. As anticipated, RF2 reacted efficiently with both complexes (MKX and MNX), releasing the dipeptide with a rate constant (k_{cat}) close to that previously reported in buffer A ($\sim 0.05 \text{ s}^{-1}$, Fig. 1c)^{13,14}. Notably, titration experiments indicated that less RF2 was required to promote the maximal rate of catalysis on the mismatched P site complex than on the matched one ($K_{1/2}$, release factor concentration at which half of the maximal rate is observed, values of $\sim 75 \text{ nM}$ and 800 nM , respectively, Fig. 1d). These data suggested that RF2 interacts differently with these two complexes that vary by a single mismatch in the P site. We note that the maximal rate of release on other matched stop-codon-programmed complexes was, as expected, dependent on the buffer used and on the source of RF2 (over- or chromosomally-expressed) reaching a maximum of 10 s^{-1} , close to numbers reported previously¹⁵ (Supplementary Fig. 3). Although maximal rates of release are achieved in buffer D, we chose to complete the study in buffer A because background release rates were minimal under these conditions.

¹Howard Hughes Medical Institute, Department of Molecular Biology and Genetics, Johns Hopkins University School of Medicine, Baltimore, Maryland 21205, USA.



Infrared laser-mediated gene induction in targeted single cells *in vivo*

Yasuhiro Kamei^{1,2,8}, Motoshi Suzuki^{3,8}, Kenjiro Watanabe^{4,8}, Kazuhiro Fujimori², Takashi Kawasaki², Tomonori Deguchi², Yoshihiro Yoneda⁵, Takeshi Todo^{1,6}, Shin Takagi³, Takashi Funatsu^{4,7} & Shunsuke Yuba²

We developed infrared laser-evoked gene operator (IR-LEGO), a microscope system optimized for heating cells without photochemical damage. Infrared irradiation causes reproducible temperature shifts of the *in vitro* microenvironment in a power-dependent manner. When applied to living *Caenorhabditis elegans*, IR-LEGO induced heat shock-mediated expression of transgenes in targeted single cells in a more efficient and less deleterious manner than a 440-nm dye laser and elicited physiologically relevant phenotypic responses.

Heat stress induces transcription of genes encoding heat shock proteins^{1–3}. In transgenic organisms this response is exploited to manipulate gene expression *in vivo*, using heat as a trigger to induce expression of a gene cloned downstream of a heat shock promoter. Moreover, by irradiating living specimens with a laser beam under a microscope, it is possible to induce genes that are under the control of a heat shock promoter in individual targeted cells. This method has advantages over conventional techniques for ectopic gene expression^{4–9}. First, it allows induction of gene expression in a specific cell without a tissue-specific promoter. Second, for induction of gene expression in different cell types, only a single strain carrying a heat shock promoter-driven transgene is required. Most importantly, it enables the induction of gene expression in single targeted cells at a defined time.

A cell-ablation microscope system with a pulsed 440-nm dye laser has previously been used for inducing gene expression mediated by the heat shock response^{4–7}. Although gene expression can be induced with a 440-nm laser^{4–7} or other visible lasers^{8,9}, leading to relevant phenotypic responses in irradiated cells^{5,7}, relatively long irradiation times are required for gene induction,

and irradiation often has detrimental effects on cells^{5,9}. Here we report an application of an infrared (IR) laser for heat shock response-mediated gene expression using a newly developed microscope system called IR-LEGO (Fig. 1a). The wavelength of IR (1,480 nm; Fig. 1a) matches the combination of symmetric and antisymmetric OH stretching modes of water and can heat water with $\sim 10^5$ -fold higher efficiency than the 440-nm laser.

To evaluate the utility of IR-LEGO, we first examined its *in vitro* heating profiles: time course of temperature changes, controllability of heating and spatial distribution of heat around the laser focus. To measure microenvironmental temperature, we exploited the temperature dependence of the fluorescence intensity of fluorescent proteins. We found that fluorescence of GFP and

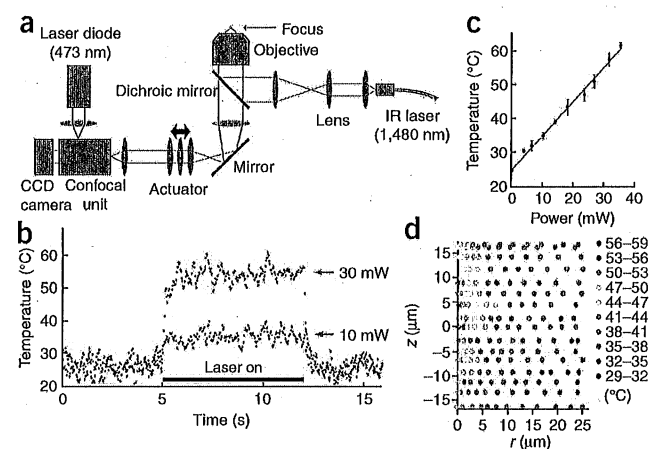


Figure 1 | Schematic illustration of microscopic system for IR-LEGO, and thermal profiles of IR-laser irradiation *in vitro*. (a) The optical path of the IR-LEGO system. The basic system used for the *in vivo* study has an IR-laser inlet path (right). For the *in vitro* study, a confocal imaging system with a fixed microscope objective (left) was additionally installed. (b) Time course of estimated temperature at the focus of the IR laser at 30 mW (red) and 10 mW (blue). Ambient temperature was 25 °C. Laser powers represent the value at the specimen plane. (c) Relationship between induced temperature and power of the IR laser. Induced temperature was the value 5 s after the start of irradiation. Ambient temperature was 25 °C. (d) Three-dimensional thermal map during IR-laser irradiation at a power of 33 mW. r , distance from the z axis; z , depth along the z axis. The position of ($r, z = 0, 0$) is the focus of the IR laser. The tissue model was irradiated from below with a laser beam of conical shape, along the z axis. The lower coverslip of the tissue model is located at $z = -18 \mu\text{m}$.

¹Radiation Biology Center, Kyoto University, Yoshida Konoe-cho, Sakyo-ku, Kyoto 606-8501, Japan. ²National Institute of Advanced and Industrial Science and Technology (AIST), 1-8-31 Midorigaoka, Ikeda, Osaka 563-8577, Japan. ³Division of Biological Science, Graduate School of Science, Nagoya University, Furo-cho, Chikusa-ku, Nagoya 464-8602, Japan. ⁴Major in Bioscience and Biomedical Engineering, Waseda University, 3-4-1 Okubo, Shinjuku, Tokyo 169-8855, Japan. ⁵Department of Cell Biology and Neuroscience, Graduate School of Medicine, Osaka University, 2-2 Yamada-oka, Suita, Osaka 565-0871, Japan. ⁶Department of Radiation Biology and Medical Genetics, Graduate School of Medicine, Osaka University, 2-2 Yamada-oka, Suita, Osaka 565-0871, Japan. ⁷Laboratory of Bio-Analytical Chemistry, Graduate School of Pharmaceutical Sciences, The University of Tokyo, 7-3-1 Hongo, Bunkyo, Tokyo 113-0033, Japan. ⁸These authors contributed equally to this work. Correspondence should be addressed to Y.K. (ykamei@radbio.med.osaka-u.ac.jp) or S.Y. (s-yuba@aist.go.jp).

Journal home > Archive > Table of Contents > Article > Abstract

- Journal home**
- Advance online publication**
- Current issue**
- Archive**
- Press releases**

Methagora
Focuses

Guide to authors
Online submission
Permissions

For referees

Free online issue

Contact the journal
Subscribe

- New Subscription
- Renew Subscription
- Paid Subscriptions
- Change of Address

naturejobs

For Advertisers

work@npg

naturereprints

About this site

For librarians

Application notes

NPG Resources

- Nature
- Nature Biotechnology
- Nature Protocols
- Nature Genetics
- Nature Chemical Biology
- Nature Cell Biology
- Nature Neuroscience

ARTICLE

Nature Methods - 4, 81 - 86 (2007)
Published online: 10 December 2006; | doi:10.1038/nmeth986

Major signal increase in fluorescence microscopy through dark-state relaxation

Gerald Donnert, Christian Eggeling & Stefan W Hell

Max Planck Institute for Biophysical Chemistry, Department of NanoBiophotonics, Am Fassberg 11, 37077 Göttingen, Germany.

Correspondence should be addressed to Stefan W Hell shell@gwdg.de

We report a substantial signal gain in fluorescence microscopy by ensuring that transient molecular dark states with lifetimes >1 μ s, such as the triplet state relax between two molecular absorption events. For GFP and Rhodamine dye Atto532, we observed a 5–25-fold increase in total fluorescence yield before molecular bleaching when strong continuous-wave or high-repetition-rate pulsed illumination was replaced with pulses featuring temporal pulse separation >1 μ s. The signal gain was observed both for one- and two-photon excitation. Obeying dark or triplet state relaxation in the illumination process signifies a major step toward imaging with low photobleaching and strong fluorescence fluxes.

Please visit methagora to view and post comments on this article

MORE ARTICLES LIKE THIS

These links to content published by NPG are automatically generated.

NEWS AND VIEWS

Lasers and the Lamb shift
Nature News and Views (25 Dec 1975)

RESEARCH

Major signal increase in fluorescence microscopy through dark-state relaxation
Nature Methods Article

STED microscopy with continuous wave beams
Nature Methods Brief Communication (01 Nov 2007)

Nonlinear magic: multiphoton microscopy in the biosciences
Nature Biotechnology Research (01 Nov 2003)

[See all 59 matches for Research](#)

Molecular Cloning
An online manual of searchable protocols. Full text access provided.

Abstract

◀ Previous | Next ▶

▶ Table of contents

Full text

Download PDF

Send to a friend

Rights and permissions

Order commercial reprints
CrossRef lists 18 articles citing this article

Save this link

▶ Figures & Tables

▼ Products

▶ Export citation

nature jobs

Senior Research Fellow

University of Southampton - Oceanography
Southampton United Kingdom

Group Leader / Scientist - Microbiology

Vimta Labs Limited
Hyderabad, Andhra Pradesh 500 051 India

[More science jobs](#)

[Post a job for free](#)

natureproducts

Search buyers guide:

Go

Evolution of cooperation through the heterogeneity of random networks

Stephen Devlin¹ and Thomas Treloar²

¹*Mathematics Department, University of San Francisco 2130 Fulton Street, San Francisco, California 94117, USA*

²*Mathematics Department, Hillsdale College 33 East College Street, Hillsdale, Michigan 49242, USA*

(Received 5 August 2008; published 21 January 2009)

We use the standardized variance (ν_{st}) of the degree distribution of a random network as an analytic measure of its heterogeneity. We show that ν_{st} accurately predicts, quantitatively, the success of cooperators in an evolutionary prisoner's dilemma. Moreover, we show how the generating functional expression for ν_{st} suggests an intrinsic interpretation for the heterogeneity of the network that helps explain local mechanisms through which cooperators thrive in heterogeneous populations. Finally, we give a simple relationship between ν_{st} , the cooperation level, and the epidemic threshold of a random network that reveals an appealing connection between epidemic disease models and the evolutionary prisoner's dilemma.

DOI: 10.1103/PhysRevE.79.016107

PACS number(s): 89.75.Hc, 87.23.Kg, 02.50.Lc, 89.75.Fb

I. INTRODUCTION

The versatility of the prisoner's dilemma (PD) as a relevant paradigm for interdisciplinary problems involving the study of conflict and cooperation has led to a vast body of research [1–6]. Indeed, the PD has become a standard tool in biology, economics, the social sciences, physics, and mathematics in which to study cooperation phenomena [1–7]. A great deal of recent attention has focused on a deepening understanding, via the evolutionary PD, of how and why cooperative behavior can emerge, thrive, and even dominate in certain frameworks despite a clear temptation for individuals to maximize their own fitness by acting selfishly [2–5,7].

In its simplest form, the PD pits two agents against each other. Agents simultaneously choose between two strategies: *C* for cooperate and *D* for defect. The essence of the game is captured in the payoffs associated with the four possible states. Setting $b > 1 > 0 \geq a$, PD payoffs are distributed according to the normalized symmetric matrix (where payoffs go to the row-player):

	<i>C</i>	<i>D</i>
<i>C</i>	1	<i>a</i>
<i>D</i>	<i>b</i>	0

(1)

It is clear from the payoff inequalities that a rational (self-interested) agent choosing independently has no incentive to play *C*. Indeed, the Nash equilibrium predicts that both agents will defect. The dilemma arises from the inefficiency of the equilibrium: both players could benefit (i.e., enjoy higher payoffs than at equilibrium) via mutual cooperation [3].

The PD has been further studied in the setting of evolutionary replicator dynamics. In this context, a strategy spreads in a population according to its fitness and the repeated interactions between agents are assumed to be random and well mixed—any agent is equally likely to interact with any other agent in the population. In such a setting, cooperation vanishes over time and the (evolutionarily stable) equilibrium rests with all agents defecting [3].

Abandoning the well-mixed scenario led to important advances. In the seminal work of Nowak and May [8], agents playing an evolutionary PD were placed at vertices in a lattice, with interactions limited to neighbors (vertices connected by edges). It was found that a nontrivial population of cooperators could become evolutionarily stable over some game parameter values.

This work led to the recognition that agent-agent interactions could be better modeled by introducing topological constraints on a population in the form of a graph, with vertices representing agents and edges indicating a relationship along which an interaction can take place. The subsequent result that spatial structure could drive cooperation in the evolutionary PD sparked intense study of the effects of varied network topologies on cooperation phenomena.

More recently [9–17], considerable attention has been given to the (discrete replicator) dynamics of an evolutionary PD on a network. Of particular interest is the now well-established result that so-called scale-free distributions (where the degrees of vertices follow a power-law distribution) greatly benefit cooperation in the PD, as well as variants like the snowdrift game. In fact, cooperation can dominate on the network over all parameter values of the game on certain networks such as the Barbási-Albert scale-free network generated via growth and preferential attachment [10].

The distinguishing characteristic of power-law distributions is that they are “heterogeneous;” the connectivity of individual agents varies widely across the network [18–20]. Many factors ultimately influence the complex dynamics of an evolutionary game on such networks, but it is well-established that heterogeneity in particular enhances the ability of cooperators to survive and thrive. While progress has been made in understanding the particulars of these complex dynamics [9], many questions remain.

This paper studies a quantifiable measure of heterogeneity that accords well with cooperation phenomena in the sense that more heterogeneity corresponds to more cooperation in an evolutionary PD in an explicit and predictable way. Also, a further explanation as to the mechanisms through which heterogeneity fosters enhanced cooperation is given. A primary focus, therefore, is on the influence of the degree distribution of a network on cooperation phenomena, which is

Fluctuations in protein synthesis from a single RNA template: Stochastic kinetics of ribosomes

Ashok Garai,^{1,*} Debashish Chowdhury,¹ and T. V. Ramakrishnan^{2,3,1}

¹Department of Physics, Indian Institute of Technology, Kanpur 208016, India

²Department of Physics, Banaras Hindu University, Varanasi 221005, India

³Department of Physics, Indian Institute of Science, Bangalore 560012, India

(Received 2 May 2008; revised manuscript received 28 November 2008; published 21 January 2009)

Proteins are polymerized by cyclic machines called ribosomes, which use their messenger RNA (mRNA) track also as the corresponding template, and the process is called translation. We explore, in depth and detail, the stochastic nature of the translation. We compute various distributions associated with the translation process; one of them—namely, the dwell time distribution—has been measured in recent single-ribosome experiments. The form of the distribution, which fits best with our simulation data, is consistent with that extracted from the experimental data. For our computations, we use a model that captures both the mechanochemistry of each individual ribosome and their steric interactions. We also demonstrate the effects of the sequence inhomogeneities of real genes on the fluctuations and noise in translation. Finally, inspired by recent advances in the experimental techniques of manipulating single ribosomes, we make theoretical predictions on the force-velocity relation for individual ribosomes. In principle, all our predictions can be tested by carrying out *in vitro* experiments.

DOI: 10.1103/PhysRevE.79.011916

PACS number(s): 87.16.dj, 87.16.af, 87.16.Nn

I. INTRODUCTION

A genetic message, chemically encoded in the DNA, is first *transcribed* into a messenger RNA (mRNA) from which it is then *translated* into proteins [1]. Both mRNA and proteins are linear polymers of monomeric subunits called nucleotide and amino acid, respectively. The genetic code contained in the sequence of codons (triplets of nucleotides) on an mRNA is translated into the corresponding sequence of amino acids by a macromolecular machine, called ribosome [2–4]. A ribosome is a cyclic machine. Each mechanochemical cycle of this machine consists of several steps which result in the translocation of the ribosome by one codon on the mRNA template and the elongation of the protein by one amino acid. Thus, the mRNA template also serves as the track for motorlike movement of the ribosome during translation [5,6]. In fact, a ribosome is like a mobile “workshop” which moves on an mRNA track and provides a platform where a coordinated action of many devices take place for the synthesis of each of the proteins.

Only a few papers over the last few years have reported results of single-ribosome imaging and manipulation [7–12]. These experiments have established that in each mechanochemical cycle, the dwell time of a ribosome at any codon is random. Moreover, this dwell time is a sum of two time intervals: namely, (i) the duration for which it makes a mechanical pause and (ii) the time it takes to translocate to the next codon.

In this paper we report our results on the dwell time distribution [12], which characterizes the stochastic translocation-and-pause dynamics of the ribosomes in a theoretical model of translation. We also introduce a few statistical distributions which characterize some other aspects of the stochastic nature of translation. We compute all these

statistical distributions by carrying out computer simulations of a model of protein synthesis that captures both the mechanochemistry of each individual ribosome, as it moves on the mRNA template, as well as their *in situ* steric interactions [13]. This model provides a “unified” description of the stochastic dynamics of ribosomes within a single theoretical framework. In the low-density limit, it accounts essentially for the translocation-and-pause dynamics of single ribosomes because the ribosomes on the mRNA track are well separated and operate practically independent of each other. On the other hand, it also predicts the effects of steric interactions of the ribosomes on the translocation-and-pause dynamics and the emergent collective properties of the ribosomes at higher densities.

This paper is organized as follows: We present our model in Sec. II and explain how it captures the essential features of ribosome traffic on a single mRNA track. In the same section, we also describe the numerical scheme we have used for computer simulations of this model. We report the results obtained from these simulation in Sec. III. We compare some of our results with the corresponding experimental observations reported earlier in the literature and discuss ways of analyzing the data. We summarize the main results and draw conclusions in Sec. IV.

II. MODEL

Almost all the earlier works on the collective operation of ribosomes on a single mRNA track [14–24] treat ribosome traffic as a problem of nonequilibrium statistical mechanics of a system of interacting “self-driven” hard rods. But strictly speaking, a ribosome is neither a particle nor a hard rod; its mechanical movement along the mRNA track is coupled to its internal mechanochemical processes, which drive the synthesis of the protein. Thus, these earlier models could not account for the effects of the intraribosome chemical and conformational transitions on their collective spa-

*Corresponding author: garai@iitk.ac.in

Facilitated Variation: How Evolution Learns from Past Environments To Generalize to New Environments

Merav Parter¹, Nadav Kashtan¹, Uri Alon*

Department of Molecular Cell Biology, Weizmann Institute of Science, Rehovot, Israel

Abstract

One of the striking features of evolution is the appearance of novel structures in organisms. Recently, Kirschner and Gerhart have integrated discoveries in evolution, genetics, and developmental biology to form a theory of facilitated variation (FV). The key observation is that organisms are designed such that random genetic changes are channeled in phenotypic directions that are potentially useful. An open question is how FV spontaneously emerges during evolution. Here, we address this by means of computer simulations of two well-studied model systems, logic circuits and RNA secondary structure. We find that evolution of FV is enhanced in environments that change from time to time in a systematic way; the varying environments are made of the same set of subgoals but in different combinations. We find that organisms that evolve under such varying goals not only remember their history but also generalize to future environments, exhibiting high adaptability to novel goals. Rapid adaptation is seen to goals composed of the same subgoals in novel combinations, and to goals where one of the subgoals was never seen in the history of the organism. The mechanisms for such enhanced generation of novelty (generalization) are analyzed, as is the way that organisms store information in their genomes about their past environments. Elements of facilitated variation theory, such as weak regulatory linkage, modularity, and reduced pleiotropy of mutations, evolve spontaneously under these conditions. Thus, environments that change in a systematic, modular fashion seem to promote facilitated variation and allow evolution to generalize to novel conditions.

Citation: Parter M, Kashtan N, Alon U (2008) Facilitated Variation: How Evolution Learns from Past Environments To Generalize to New Environments. *PLoS Comput Biol* 4(11): e1000206. doi:10.1371/journal.pcbi.1000206

Editor: Gary Stormo, Washington University, United States of America

Received: February 19, 2008; **Accepted:** September 16, 2008; **Published:** November 7, 2008

Copyright: © 2008 Parter et al. This is an open-access article distributed under the terms of the Creative Commons Attribution License, which permits unrestricted use, distribution, and reproduction in any medium, provided the original author and source are credited.

Funding: NIH and the Kahn Family.

Competing Interests: The authors have declared that no competing interests exist.

* E-mail: urialon@weizmann.ac.il

☉ These authors contributed equally to this work.

Introduction

The origin of the ability to generate novelty is one of the main mysteries in evolution. Pioneers of evolutionary theory, including Baldwin [1], Simpson [2], and Waddington [3,4], suggested how useful novelty might be enhanced by physiological adaptations and by the robustness of the developmental process. These early theories were limited by a lack of knowledge of the molecular mechanisms of development.

Recent decades saw breakthroughs in the depth of understanding of molecular and developmental biology. Many of these findings were unified in the theory of facilitated variation [5], presented by Kirschner and Gerhart, that addresses the following question: how can small, random genetic changes be converted into complex useful innovations? In order to understand novelty in evolution, Kirschner and Gerhart integrated observations on molecular mechanisms to show how the current design of an organism helps to determine the nature and the degree of future variation. The key observation is that the organism, by its intrinsic construction, biases both the type and the amount of its phenotypic variation in response to random genetic mutation [3,4,6–10]. In other words, the organism seems to be built in such a way that small genetic mutations have a high chance of yielding a large phenotypic payoff.

To understand FV, it is important to compare it to the related concept of evolvability. A biological system is evolvable if it can

readily acquire novel functions through genetic changes that help the organism survive and reproduce in future environments [11]. Evolvability is composed of two aspects: 1) variability: the capacity to generate new phenotypes 2) fitness: the fitness of the new phenotypes in future environments. Most studies of evolvability focused on the first aspect, variability. Such studies measured the range and diversity of the phenotypic variation that can be generated by a given mutation, usually without discerning between potentially useful phenotypes and non-useful ones [12–16] (for an interesting exception see Ciliberti et al [17]). FV theory adds to previous considerations by focusing on the nature of the generated variation, and specifically on the organism's ability to generate novel phenotypes which are potentially *useful*.

Facilitated variation (FV) is made possible by certain features of biological design. One of these is the existence of 'weak regulatory linkage' [5,10,18], where general and non-instructive signals can trigger large pre-prepared responses. For example, changes in growth hormone concentration at a localized position (limb bud in an embryo) can trigger large useful changes in the shape of the limb, driven by the conserved mechanisms for growth of bones, muscles, blood vessels, and nerves [19]. A good example is the ease of changing beak shapes with any of many possible mutations that affect the concentration of a single morphogenetic factor [20] (Figure 1A). In weak regulatory linkage, the information about the output is pre-built into the regulated system without instruction from the regulator, which only selects between states. Such

Exploration dynamics in evolutionary games

Arne Traulsen^{a,b,1}, Christoph Hauert^{b,c}, Hannelore De Silva^d, Martin A. Nowak^b, and Karl Sigmund^{e,f}

^aMax Planck Institute for Evolutionary Biology, D-24306 Plön, Germany; ^bProgram for Evolutionary Dynamics, Harvard University, Cambridge, MA 02138; ^cDepartment of Mathematics, University of British Columbia, Vancouver, BC, Canada V6T 1Z2; ^dVienna University of Economics and Business Administration, A-1090 Vienna, Austria; ^eFaculty of Mathematics, University of Vienna, A-1090 Vienna, Austria; and ^fInternational Institute for Applied Systems Analysis, A-2361 Laxenburg, Austria

Edited by Simon A. Levin, Princeton University, Princeton, NJ, and approved November 21, 2008 (received for review August 28, 2008)

Evolutionary game theory describes systems where individual success is based on the interaction with others. We consider a system in which players unconditionally imitate more successful strategies but sometimes also explore the available strategies at random. Most research has focused on how strategies spread via genetic reproduction or cultural imitation, but random exploration of the available set of strategies has received less attention so far. In genetic settings, the latter corresponds to mutations in the DNA, whereas in cultural evolution, it describes individuals experimenting with new behaviors. Genetic mutations typically occur with very small probabilities, but random exploration of available strategies in behavioral experiments is common. We term this phenomenon "exploration dynamics" to contrast it with the traditional focus on imitation. As an illustrative example of the emerging evolutionary dynamics, we consider a public goods game with cooperators and defectors and add punishers and the option to abstain from the enterprise in further scenarios. For small mutation rates, cooperation (and punishment) is possible only if interactions are voluntary, whereas moderate mutation rates can lead to high levels of cooperation even in compulsory public goods games. This phenomenon is investigated through numerical simulations and analytical approximations.

cooperation | costly punishment | finite populations | mutation rates

Evolutionary game dynamics describes how successful strategies spread in a population (1, 2). Individuals receive a payoff from interactions with others. Those strategies that obtain the highest payoffs have the largest potential to spread in the population, either by genetic reproduction or by cultural imitation. For example, from time to time, a random focal individual could compare its payoff with another, randomly chosen role model. The role model serves as a benchmark for the focal individual's own strategy. Depending on the payoff comparison, the focal individual either sticks to its old strategy or it imitates the role model's strategy. We focus here on the simplest choice for a payoff comparison, which is the following imitation dynamics (3): If the role model has a higher payoff, the focal individual switches to the role model's strategy. If the role model has a lower payoff, the focal individual sticks to its own strategy. If both payoffs are identical, it chooses between the 2 strategies at random. The imitation dynamics can be obtained from other dynamics with probabilistic strategy adoption in the limit of strong selection (4). When only 2 strategies are present, the dynamics becomes deterministic in following the gradient of selection. In infinite populations, it leads to deterministic dynamics closely related to the classical replicator equation (5, 6). In both cases, the dynamics remains stochastic if the payoff differences vanish. For large populations and in the absence of mutations, the replicator dynamics is a useful framework to explore the general dynamics of the system. However, because it does not include any stochastic terms, it is not necessarily a good approach to describe the dynamics in behavioral experiments. In finite populations, the system is affected by noise, which can trigger qualitative changes in the dynamics.

Although imitation dynamics are a common way to model evolutionary game dynamics, they do not include the possibility

to explore the available strategies. Thus, we allow for random exploration (or mutations) in addition to the imitation dynamics. In our model, mutations occur with probability μ in each update step. In genetic settings, mutations change the strategy encoded in the genome. In such a setting, the mutation probabilities μ are expected to be small. In contrast, according to behavioral experiments (8, 9), the willingness of humans to explore strategic options implies much higher mutation rates. In such settings, people not only imitate others but also act emotionally, attempt to outwit others by anticipating their actions, or just explore their strategic options (7–9). As a first approximation for a system with few strategies, we subsume the occurrence of such behavior by a large exploration rate, which leads to the continuous presence of all strategic types. For example, in compulsory public goods games without punishment, $\approx 20\%$ of the players cooperate (M. Milinski, personal communication), even though defection is dominant. Therefore, it seems reasonable to consider mutation rates even greater than 10%.

Thus, 2 limiting cases can be considered: Either random exploration represents a small disturbance to a pure imitation process ($\mu \ll 1$) or imitation is a weak force affecting a purely random choice process ($1 - \mu \ll 1$). This second limit is a simple way to incorporate effects that cannot be captured by imitation. For both cases, we present analytical approximations.

To make our analysis more concrete, we focus on the evolution of cooperation, which is a fascinating problem across disciplines such as anthropology, economics, evolutionary biology, and social sciences (10, 11). In public goods games among N players, cooperation sustains a public resource. Contributing cooperators pay a cost c to invest in a common good (12, 13). All contributions are summed up, multiplied by a factor r ($1 < r < N$) and distributed among all participants, irrespective of whether they contributed or not. Because only a fraction $r/N < 1$ of the focal individual's own investment is recovered by the investor, it is best to defect and not to contribute. This generates a social dilemma (14): Individuals that "free ride" on the contributions of others and do not invest perform best. Such behavior spreads, and no one invests anymore. Consequently, the entire group suffers, because everyone is left with zero payoff instead of $c(r - 1)$ (15). This outcome changes if individuals can identify and punish defectors. Punishment is costly and means that one individual imposes a fine on a defecting coplayer (7, 16–21). The establishment of such costly behavior is not trivial (22, 23): A single punishing cooperator performs poorly in a population of defectors. Moreover, punishment is not stable unless there are sanctions also on those who cooperate but do not punish. Otherwise, such "second-order free riders" can under-

Author contributions: A.T., C.H., H.D.S., M.A.N., and K.S. designed research, performed research, analyzed data, and wrote the paper.

The authors declare no conflict of interest.

This article is a PNAS Direct Submission.

¹To whom correspondence should be addressed. E-mail: traulsen@evolbio.mpg.de.

This article contains supporting information online at www.pnas.org/cgi/content/full/0808450106/DCSupplemental.

© 2009 by The National Academy of Sciences of the USA

A DNA damage response in *Escherichia coli* involving the alternative sigma factor, RpoS

Houra Merrikh^a, Alexander E. Ferrazzoli^a, Alexandre Bougdour^b, Anique Olivier-Mason^a, and Susan T. Lovett^{a,1}

^aDepartment of Biology and Rosenstiel Basic Medical Sciences Center, Brandeis University, Waltham, MA 02254-9110; and ^bLaboratory of Molecular Biology, National Cancer Institute, National Institutes of Health, Bethesda, MD 20892

Edited by Nancy Kleckner, Harvard University, Cambridge, MA, and approved November 21, 2008 (received for review April 16, 2008)

We isolated an *Escherichia coli* mutant in the *iraD* gene, sensitive to various forms of DNA damage. Our data are consistent with the function of IraD to promote accumulation of the alternative transcription sigma factor, RpoS, by binding to the adaptor RssB protein that targets RpoS for degradation. Our results demonstrate the physiological importance of this mode of regulation for DNA damage tolerance. Although RpoS is best known for its regulation of genes induced in stationary phase, our work underscores the importance of the RpoS regulon in a DNA damage response in actively growing cells. We show that *iraD* transcription is induced by DNA damage by a mechanism independent of the SOS response. The IraD and SOS regulatory pathways appear to act synergistically to ensure survival of cells faced with oxidative or DNA damaging stress during cellular growth.

oxidative stress | posttranslational regulation | replication stress | SOS response | DNA repair

Throughout its life cycle, *Escherichia coli* is faced with different environmental challenges and regulates gene expression accordingly. One way is by changes in the promoter recognition of RNA polymerase via different situation-specific σ factors (1). In *E. coli*, the major alternative sigma factor is σ S (RpoS), which is required for expression of specific genes on entry to stationary phase or as a response to stress (2–4). Although the RpoS dependence of many of these responses and the regulation of RpoS itself have been well studied, the relevance of this to DNA repair has not been a major focus.

To find genes important in DNA damage responses, we performed a random Tn5 transposon insertion mutant screen, assaying sensitivity to, among other agents, phleomycin and azidothymidine (AZT). Phleomycin induces random single- or double-strand breaks in the backbone of DNA (5), whereas AZT blocks DNA synthesis, leading to single-strand gaps in the replication fork (6). One insertion mutant in *iraD* (previously an unknown gene, *yjiD*) was hypersensitive to phleomycin and AZT.

Recent work from Gottesman and coworkers (7) implicated IraD in posttranslational regulation of RpoS. The RssB adaptor protein targets RpoS to ClpXP for degradation during logarithmic growth, keeping RpoS protein levels low in the absence of stress (8–12). IraD was identified in a high-copy plasmid screen for genes promoting accumulation of an RpoS-LacZ fusion protein. The IraD gene product acts as an antiadaptor protein via direct binding and inhibition of the ability of RssB to target RpoS for proteolysis by ClpXP *in vitro* (7).

In the work presented here, we demonstrate that IraD is required for survival to DNA damage, providing evidence of the physiological importance of IraD in particular and the antiadaptor mechanism in general. The data presented suggest that IraD acts as an antagonist of RssB, regulating RpoS levels and stabilization, not only after DNA damage but constitutively. Our results establish the importance of RpoS stabilization in proliferating bacterial cells in which replication has been directly blocked, confirming a role for the RpoS regulon in DNA damage repair or tolerance. This model of regulation via protein stabilization may allow rapid and transient induction of the RpoS

regulon. We demonstrate induction of *iraD* by various forms of DNA damage by a mechanism independent of the SOS response. The loss of both IraD and SOS responses leads to a synergistic decrease in the ability to withstand DNA damage, indicating that both pathways function in a complementary fashion to ensure cell survival.

Results

Isolation and Characterization of an *iraD* Transposon Insertion Allele.

To identify DNA damage response factors in *E. coli*, we mutagenized cells by random insertion of Tn5-EZ and screened for hypersensitivity to DNA damaging agents. One insertion mutant showing hypersensitivity to both AZT and phleomycin mapped to the ORF, *iraD*. Sequence analysis revealed an insertion 18 nt downstream from the ATG start site, followed by a 9-nt target site duplication. The orientation of the Tn5 element was such that the *kan* promoter could potentially transcribe an IraD protein truncated by 3 amino acids at its N terminus. Because of the possibility that the Tn5 allele does not completely inactivate IraD function and could disrupt its regulation, we also examined a complete deletion, *iraDA*, in the analysis that follows.

IraD Is Important for Survival of DNA Damage in Growing Cells. In a microarray study, *iraD* transcripts were induced almost 30-fold after hydrogen peroxide treatment, ranking as the seventh highest *E. coli* gene up-regulated after oxidative stress (13). We found that the original *iraD::Tn5* and the *iraDA* mutant were extremely sensitive to hydrogen peroxide, with a decrease in survival greater than 10-fold relative to WT strains after modest exposure (Table 1A) of early exponentially growing cultures. The *iraD::Tn5* mutant showed somewhat greater sensitivity to hydrogen peroxide than the null allele in this experiment; the basis for this finding is unknown, and this reduced sensitivity was not seen under all assay conditions.

A high-copy plasmid expressing the *iraD* gene from its natural promoter fully complemented peroxide sensitivity of the *iraDA* mutant, whereas expressing just the promoter region of *iraD* did not (Table 1B). (The Tn5 allele could not be tested because it already carries the *kan* resistance gene for the plasmid.) At higher doses of peroxide, a lower copy ampicillin-resistance plasmid expressing *iraD* from its natural promoter only partially complemented the *iraDA* strain, although it fully complemented the *iraD::Tn5* allele (Fig. 1). The difference between the two alleles confirms our suspicion that *iraD::Tn5* is not a null allele; incomplete complementation of the null allele may result from failure to express sufficient plasmid-encoded *iraD*⁺. In addition, we used P1 phage transduction to replace the mutant copy of *iraD* with a WT copy of the gene in both mutant strain

Author contributions: H.M., A.E.F., and S.T.L. designed research; H.M. and A.E.F. performed research; H.M., A.E.F., A.B., and A.O.-M. contributed new reagents/analytic tools; H.M., A.E.F., and S.T.L. analyzed data; and H.M. and S.T.L. wrote the paper.

The authors declare no conflict of interest.

This article is a PNAS Direct Submission.

¹To whom correspondence should be addressed. E-mail: lovett@brandeis.edu.

© 2009 by The National Academy of Sciences of the USA

Growth-rate-dependent partitioning of RNA polymerases in bacteria

Stefan Klumpp¹ and Terence Hwa

Center for Theoretical Biological Physics and Department of Physics, University of California at San Diego, La Jolla, CA 92093-0374

Edited by José N. Onuchic, University of California at San Diego, La Jolla, CA, and approved October 27, 2008 (received for review May 21, 2008)

Physiological changes that result in changes in bacterial gene expression are often accompanied by changes in the growth rate for fast adapting enteric bacteria. Because the availability of RNA polymerase (RNAP) in cells depends on the growth rate, transcriptional control involves not only the regulation of promoters, but also depends on the available (or free) RNAP concentration, which is difficult to quantify directly. Here, we develop a simple physical model describing the partitioning of cellular RNAP into different classes: RNAPs transcribing mRNA and ribosomal RNA (rRNA), RNAPs nonspecifically bound to DNA, free RNAP, and immature RNAP. Available experimental data for *Escherichia coli* allow us to determine the 2 unknown parameters of the model and hence deduce the free RNAP concentration at different growth rates. The results allow us to predict the growth-rate dependence of the activities of constitutive (unregulated) promoters, and to disentangle the growth-rate-dependent regulation of promoters (e.g., the promoters of rRNA operons) from changes in transcription due to changes in the free RNAP concentration at different growth rates. Our model can quantitatively account for the observed changes in gene expression patterns in mutant *E. coli* strains with altered levels of RNAP expression without invoking additional parameters. Applying our model to the case of the stringent response after amino acid starvation, we can evaluate the plausibility of various scenarios of passive transcriptional control proposed to account for the observed changes in the expression of rRNA and biosynthetic operons.

constitutive promoters | ribosomal RNA | stringent response | transcription

Bacteria are able to grow with wildly different growth rates in different media. Depending on the growth conditions, the quality and availability of nutrients, they differ in cell size and macromolecular compositions, e.g., the ratio of protein, RNA, and DNA (1, 2). For bacteria in exponential growth phase, this dependence was found empirically as a dependence on *growth rate* rather than as a dependence on the specific growth medium, because bacteria grown in different media that support the same growth rate exhibited the same macromolecular composition (1–3). For this reason, many parameters of the bacterial cell have been characterized as functions of the growth rate (4). Many of these parameters affect gene expression, e.g., the cellular abundance of transcription and translation machinery. Gene expression is therefore expected to exhibit a generic growth-rate dependence in addition to the specific genetic regulation (5). Indeed, even unregulated (or “constitutively expressed”) promoters exhibit growth-rate-dependent activities (5, 6). Some genes, e.g., the ribosomal RNA operons (*rnn*), are additionally regulated in a growth-rate-dependent fashion (7, 8).

One difficulty in elucidating various mechanisms of growth-rate-dependent transcriptional control lies in the fact that the activity of a promoter depends not only on the active control mechanisms, but also directly on the availability of RNA polymerase (RNAP), which is growth-rate dependent. For example, the total number of RNAPs per cell was determined to increase from 1,500 at slow growth (0.6 doublings per hour) to 11,400 at fast growth (2.5 doublings per hour) (4). How the concentration of *free* RNAPs, which is crucial to the initiation of transcription, depends on growth rate is less clear. Nevertheless, “passive transcriptional control” (3), i.e.,

changes in gene expression due to changes of the free RNAP concentration alone, was proposed to play a role in the growth-rate-dependent regulation of rRNA transcription (7, 9), based on observations that similar behaviors could be induced by RNAP mutations (9, 10). Passive control has also been proposed to account for changes in transcription on sudden depletion of nutrients, during the so-called “stringent response.” Surprisingly, both decreasing and increasing free RNAP concentrations have been proposed to occur during the stringent response, and were invoked by different authors to explain either the down-regulation of *rnn* operons (6, 9) or the up-regulation of biosynthetic operons (10, 11). These proposals are hard to test experimentally, because the concentration of the free RNAPs in cells is difficult to measure directly. Also, indirect inference based on measurements of the cytoplasmic fraction of RNAPs (12, 13) and promoter activities (6, 14) rely on assumptions that may be questioned (see below).

In this study, we developed a method to estimate the free RNAP concentration in *Escherichia coli* cells growing with different growth rates. Our method is based on a physical model that partitions the RNAPs in a cell into fractions representing RNAPs transcribing mRNA and rRNA, RNAPs nonspecifically bound to DNA, free RNAPs, and RNAP assembly intermediates. Our model combined features from previous studies of RNAP partitioning (15–17), none of which, however, included all of these fractions. By integrating the available data from both direct and indirect measurements of the free RNAP concentration with the growth-rate dependence of the macromolecular composition of *E. coli* cells (4), this model allowed us to predict the growth-rate-dependent partitioning of RNAPs, thereby providing a quantitative picture of the various activities of RNAPs in the cell. The results for the concentration of free RNAP allowed us to predict the growth-rate dependence of the activities of the constitutive promoters, as well as to disentangle the various growth-rate-dependent factors affecting the activity of the *rnn* promoters. We finally applied our model to investigate the change in free-RNAP concentration during the stringent response and test several scenarios for passive control. The results suggest that passive control, both positive and negative, should not be expected to play a major role in the stringent response, at least in the early stage immediately after sudden starvation.

Model and Results

The concentration of free RNAPs in cells is difficult to measure. Two approaches have been described in the literature. The first one is indirect and uses transcription from a constitutive (unregulated) promoter (6, 7, 14, 18). This approach yields only RNAP concentrations relative to the Michaelis constant of that

Author contributions: S.K. and T.H. designed research; S.K. performed research; and S.K. and T.H. wrote the paper.

The authors declare no conflict of interest.

This article is a PNAS Direct Submission.

¹To whom correspondence should be addressed. E-mail: klumpp@ctbp.ucsd.edu.

This article contains supporting information online at www.pnas.org/cgi/content/full/0804953105/DCSupplemental.

© 2008 by The National Academy of Sciences of the USA

Deadly competition between sibling bacterial colonies

Avraham Be'er^{a,1}, H. P. Zhang^a, E.-L. Florin^a, Shelley M. Payne^b, Eshel Ben-Jacob^{c,1}, and Harry L. Swinney^{a,1}

^aCenter for Nonlinear Dynamics and Department of Physics and ^bSection for Molecular Genetics and Microbiology, University of Texas, Austin, TX 78712; and ^cSchool of Physics and Astronomy, Raymond and Beverly Sackler Faculty of Exact Sciences, Tel Aviv University, Tel Aviv 69978, Israel

Contributed by Harry L. Swinney, November 26, 2008 (sent for review September 22, 2008)

Bacteria can secrete a wide array of antibacterial compounds when competing with other bacteria for the same resources. Some of these compounds, such as bacteriocins, can affect bacteria of similar or closely related strains. In some cases, these secretions have been found to kill sibling cells that belong to the same colony. Here, we present experimental observations of competition between 2 sibling colonies of *Paenibacillus dendritiformis* grown on a low-nutrient agar gel. We find that neighboring colonies (growing from droplet inoculation) mutually inhibit growth through secretions that become lethal if the level exceeds a well-defined threshold. In contrast, within a single colony developing from a droplet inoculation, no growth inhibition is observed. However, growth inhibition and cell death are observed if material extracted from the agar between 2 growing colonies is introduced outside a growing single colony. To interpret the observations, we devised a simple mathematical model for the secretion of an antibacterial compound. Simulations of this model illustrate how secretions from neighboring colonies can be deadly, whereas secretions from a single colony growing from a droplet are not.

bacterial competition | bacterial growth | growth inhibition | *Paenibacillus dendritiformis*

Bacteria are not the simple solitary creatures of limited capabilities they were long believed to be. When exposed to harsh environmental conditions such as starvation, hard surfaces, extreme heat, and hazardous chemicals, the bacteria can collectively develop sophisticated strategies for adaptation and survival. One aspect of this cooperative behavior is the formation of complex colonies with different spatiotemporal patterns, as needed for efficient response to the environmental conditions (1–13).

To coordinate such cooperative ventures, bacteria have developed methods of cell-to-cell signaling (14–19), including direct physical interactions by extra membrane polymers (20–21), secretion of extracellular materials like lubricating surfactin (22–23), biochemical communication such as quorum sensing and chemotaxis signaling (by using mediators ranging from simple molecules and polymers to peptides and complex proteins) (24–29), and exchange of genetic information (by plasmids and viruses) (30–32). Bacterial communication-based cooperation can lead to colony morphogenesis, coordinated gene expression, regulated cell differentiation, and division of tasks. Intercellular communication is achieved through highly complex and intricate intracellular mechanisms involving signal transduction networks (33) and gene network dynamics to turn genes on and off (34).

Bacteria competing with unrelated or distantly related strains for limited resources in the same niche cooperate to secrete antibacterial compounds to attack the competing strains (35–36). Although antibacterial compounds such as bacteriocins affect only similar or closely related bacteria, such “chemical weapons” can even be used to attack sibling cells within the same colony (37–39). An example is “fratricide” in *Streptococcus pneumoniae* (during the transition to competence) (39–41). Another example is “cannibalism” in *Bacillus subtilis*, where bacteria during the early stages of sporulation produce chemicals that kill some siblings, which become food for the surviving

bacteria (37–38). This complex behavior involves the activation of many genes and ensures the survival of the colony as a whole.

Based on these observations, one expects that there must also be competition between sibling colonies for survival. Indeed, communication between sibling colonies has been observed in a preliminary study of interaction between 2 colonies of *Paenibacillus dendritiformis*; neighboring colonies showed inhibited growth, and it was suggested, based on comparison with model simulations, that the repulsion was not simply due to food depletion but was due to mutual inhibition through some signaling factor (42–44).

In this article, we report a quantitative experimental investigation of competition between 2 growing sibling bacterial colonies. We study the Gram-positive lubricating bacterial strain *P. dendritiformis*, which develops complex colonial (bush-like) branching patterns that are sensitive to small changes in the environment when grown on nutrient-limited surfaces (9, 11, 12). The patterns slowly grow to several centimeters in diameter, which makes these bacteria ideal for studying pattern development, internal structure of branches, and mutual inhibition between 2 colonies.

Results

Competing Sibling Colonies. Two sibling colonies of *P. dendritiformis* were inoculated simultaneously on an agar plate at the same distance from the plate’s center. We refer to the colonies as “siblings” because they were taken from the same bacterial culture. The time development of such a pair of colonies (separated in distance d) is presented in Fig. 1A. The initial development of each colony is just the same as for a single isolated colony: After a lag time of ≈ 18 h, a colony starts to expand outward, developing an intricate branched pattern within a well-defined circular envelope. The speed of the growth envelope is isotropic (see Fig. 1A, 40 h) and constant, as illustrated by the straight line of white diamonds in Fig. 2A [see also supporting information (SI) Movie S1 and Movie S2]. However, after a well-defined time $\tau(d)$ when a colony has grown a distance $x_r(d)$, a colony’s front facing its neighbor starts to decelerate, and the growth front finally stops at $x_f(d)$, leaving a gap between the colonies (see Fig. 2A for different d). The final separation between colonies depends linearly on their initial separation (see Fig. 3A); this separation is smaller for larger peptone levels (Fig. 3B) and almost independent of agar concentration (Fig. 3C). These results led us initially to suspect that food depletion leads to the growth inhibition, as has been observed in studies of the growth of *B. subtilis* (45).

To distinguish between the food depletion and signaling mechanisms, we measured the diffusion constant of peptone in

Author contributions: A.B., H.P.Z., E.-L.F., S.M.P., E.B.-J., and H.L.S. designed research; A.B. performed the experiments; H.P.Z. did the mathematical modeling; A.B., H.P.Z., E.-L.F., S.M.P., E.B.-J., and H.L.S. analyzed data; and A.B., H.P.Z., E.-L.F., S.M.P., E.B.-J., and H.L.S. wrote the paper.

The authors declare no conflict of interest.

¹To whom correspondence may be addressed. E-mail: swinney@chaos.utexas.edu, abeer@chaos.utexas.edu, or eshelbj@gmail.com.

This article contains supporting information online at www.pnas.org/cgi/content/full/0811816106/DCSupplemental.

© 2009 by The National Academy of Sciences of the USA

Computation of mutual fitness by competing bacteria

Juan E. Keymer^{a,1,2}, Peter Galajda^{b,1}, Guillaume Lambert^c, David Liao^c, and Robert H. Austin^{c,d,2}

^aKavli Institute of Nanoscience, Delft University of Technology, 2628 CJ Delft, The Netherlands; ^bFaculty of Arts and Sciences Center for Systems Biology, Harvard University, Cambridge, MA 02138; ^cDepartment of Physics, Princeton University, Princeton, NJ 08544; and ^dInstitute for Advanced Study, Hong Kong University of Science and Technology, Clearwater Bay, Hong Kong

Contributed by Robert H. Austin, October 28, 2008 (sent for review August 20, 2008)

Competing populations in shared spaces with nonrenewable resources do not necessarily wage a battle for dominance at the cost of extinction of the less-fit strain if there are fitness advantages to the presence of the other strain. We report on the use of nanofabricated habitat landscapes to study the population dynamics of competing wild type and a growth advantage in stationary phase (GASP) mutant strains of *Escherichia coli* in a sealed and heterogeneous nutrient environment. Although GASP mutants are competitors with wild-type bacteria, we find that the 2 strains cooperate to maximize fitness (long-term total productivity) via spatial segregation: despite their very close genomic kinship, wild-type populations associate with wild-type populations and GASP populations with GASP populations. Thus, wild-type and GASP strains avoid each other locally, yet fitness is enhanced for both strains globally. This computation of fitness enhancement emerges from the local interaction among cells but maximizes global densities. At present we do not understand how fluctuations in both spatial and temporal dimensions lead to the emergent computation and how multilevel aggregates produce this collective adaptation.

biophysics | competition | ecology | microbiology

In business, large corporations can win temporarily by securing monopolies and driving small companies to extinction but at the cost of innovation caused by removal of competition (1). In the world of microorganisms, dominant populations that eliminate competing strains can lose ultimately if the competing strain driven to extinction can provide fitness enhancement to the dominant strain. Extinction phenomena of overexploitation for renewable resources have been characterized by the Tragedy of the Commons (2), but such extinction scenarios are not the norm in natural spatially heterogeneous habitats, at least for “lower” organisms. For example, bacteria segregate their populations into microecological niches in environments as diverse as soil (3) and coexist in a collective computation of coadaptation.

By “computation” we refer to the collective adaptive response in bacterial populations to present and/or future anticipated changes in the environment. This emergent computation (4) that optimizes global quantities from locally interacting agents has also been reported in other biological systems ranging from DNA (5) to plants (6, 7). At the simplest level, here the computation can be viewed as a process by which the global cell densities are collectively optimized (mutual fitness) by locally adapting cells. *Escherichia coli* cells have evolved sophisticated biological networks to gauge environmental conditions and to adapt to them. This can occur at the network level (8), at the epigenetic level through DNA methylation (9), and at the genomic level through mutations (10).

When bacteria are cultured in a test tube, the initial exponential growth phase leads to entry into stationary phase. After several days in this stationary phase mutant strains emerge (11). These mutants carry a growth advantage in stationary phase (GASP) phenotype: in competitive experiments, under stationary phase conditions, GASP mutants prosper at the cost of the wild-type (WT) cells (12–14). We did our competitive experiments by using (red and green) fluorescent constructs carrying rpoS WT and rpoS 819 bacteria, characterized by mutations in

the rpoS gene typically, which codes the σ_S factors of the RNA polymerase (15–17).

The switching of σ factors (from log phase σ_{38} to stationary phase σ_S) triggers the entry into stationary phase. We compared monoculture populations with 2-strain (WT and GASP) competitive communities and compared total biomass productivity across experiments.

Multispecies communities can be described by a simple Lotka–Volterra equation (Eq. 1), where the bacterial density of strain i is $\rho_i(t)$, the effective growth rate is r_i , and the influence of the strains on each other is characterized by the (community) matrix element $J_{i,j}$ that represents the ecological coupling between strains and their environment (18).

$$\frac{d\rho_i}{dt} = r_i \rho_i \left(1 - \sum_j J_{i,j} \rho_j \right) \quad [1]$$

In spatially extended systems, however, parameters of Eq. 1 vary in space and time at multiple scales in a complex manner. Critical scales are a result of the landscape structure and interactions between individuals (19, 20) and thus are difficult to determine a priori. Instead, we use an empirical approach and study the effect of landscape structure and ecological coupling experimentally. The questions we ask here are: (i) what is the influence of habitat on competition, (ii) what is the optimum fraction of WT and GASP mutant cells that maximizes fitness for the combination of WT and GASP mutants, and (iii) what is the time course approach to this solution.

Results

We built on our previous work (21) and used nanofabrication techniques to carry out molecular biology-engineered competition experiments within restricted environments with nonrenewable resources. Fig. 1 shows a diagram of the engineered structures, called microhabitat patches (MHPs), lying at the core of the experiments discussed below. The MHP array consists of 85 chambers of dimensions $100 \times 100 \times 8 \mu\text{m}$ interconnected by $5\text{-}\mu\text{m}$ -wide, $50\text{-}\mu\text{m}$ -long junction channels (JCs). Resources can diffuse into the MHPs through 200-nm deep nanoslits (NS) from nutrient reservoirs (NR) of volume ratio (MHP/NR) of 600:1. Although the JCs allow the bacteria to move between the MHPs, the NS only allow nutrients and waste to diffuse into and out of the MHPs. Many variables enter into the chip design and the experiment presented. Here, we focus on the coupling between the nutrient reservoirs and the MHPs: a nutrient landscape was created by modifying the number of NS open in each MHP. We made a simple step function of the nutrient landscape: we

Author contributions: J.E.K., P.G., G.L., D.L., and R.H.A. designed research; J.E.K., P.G., G.L., D.L., and R.H.A. performed research; J.E.K., P.G., G.L., D.L., and R.H.A. analyzed data; and J.E.K., P.G., G.L., D.L., and R.H.A. wrote the paper.

The authors declare no conflict of interest.

Freely available online through the PNAS open access option.

¹J.E.K. and P.G. contributed equally to this work.

²To whom correspondence may be addressed. E-mail: j.e.keymervergara@tudelft.nl or austin@princeton.com.

© 2008 by The National Academy of Sciences of the USA

Determination of cell fate selection during phage lambda infection

François St-Pierre^a and Drew Endy^{b,1}

Departments of ^aBiology and ^bBiological Engineering, Massachusetts Institute of Technology, Cambridge, MA 02139

Edited by Mark Ptashne, Memorial Sloan-Kettering Cancer Center, New York, NY, and approved October 8, 2008 (received for review September 5, 2008)

Bacteriophage lambda infection of *Escherichia coli* can result in distinct cell fate outcomes. For example, some cells lyse whereas others survive as lysogens. A quantitative biophysical model of lambda infection supports the hypothesis that spontaneous differences in the timing of individual molecular events during lambda infection leads to variation in the selection of cell fates. Building from this analysis, the lambda lysis-lysogeny decision now serves as a paradigm for how intrinsic molecular noise can influence cellular behavior, drive developmental processes, and produce population heterogeneity. Here, we report experimental evidence that warrants reconsidering this framework. By using cell fractionation, plating, and single-cell fluorescent microscopy, we find that physical differences among cells present before infection bias lambda developmental outcomes. Specifically, variation in cell volume at the time of infection can be used to help predict cell fate: a ≈ 2 -fold increase in cell volume results in a 4- to 5-fold decrease in the probability of lysogeny. Other cell fate decisions now thought to be stochastic might also be determined by pre-existing variation.

deterministic | extrinsic variation | lysis-lysogeny | stochastic

One of the best-studied natural biological systems for exploring cell fate commitment is bacteriophage lambda. Lambda-infected cells typically become lytic or lysogenic. Cells that become lytic produce and release progeny phage into the environment following lysis of the host cell. Alternatively, if infected cells become lysogenic, the phage genome integrates into the bacterial chromosome and the resulting prophage is passively replicated within the surviving cell and its offspring (1–3).

In studying the lambda lysis-lysogeny “decision,” a valuable starting observation is that, across many conditions, genetically identical cells grown in the same environment and each infected with a single lambda particle select different cell fates: Some cells lyse whereas other cells become lysogens (4–6). This variability in cell fate is unlikely to be due to genetic variation within the phage population or to an artifact of the experimental methods used to grow infected cells or quantify developmental outcome (Figs. S1 and S2) (4, 5). Given this observation, how do genetically identical cells infected with the same number of phage particles give rise to distinct cell fates?

In considering this question, cell fate selection during lambda infection has emerged as a paradigm for how biochemical “noise” might account for differences in developmental outcomes (7–10). In particular, Arkin and colleagues (7) used a detailed stochastic chemical kinetics model of lambda infection to analyze whether the lysis-lysogeny decision might be driven by spontaneous differences in the timing of individual biochemical reaction events. In the Arkin model, initially identical newly infected cells are expected to spontaneously accumulate quantitative differences in the abundances of key regulatory molecules, which then propagate through the lysis-lysogeny “decision circuitry” and result in distinct cell fates (Fig. 1A).

The Arkin model is important for at least 2 reasons. First, the model revitalized the study of how lambda-infected cells produce distinct cell fates, recognizing that the existing detailed descrip-

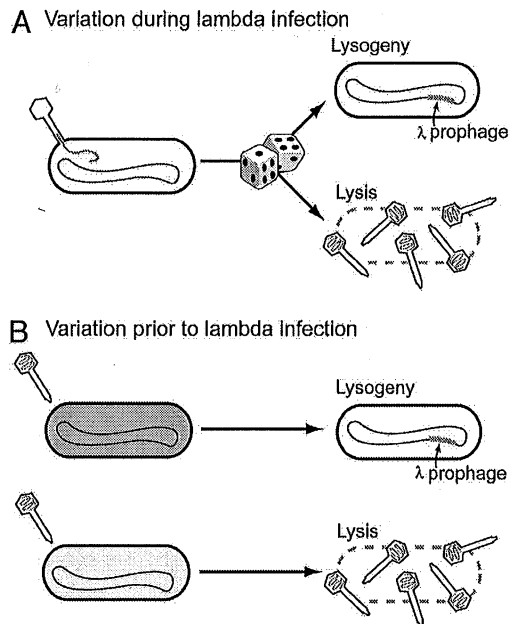


Fig. 1. Alternative models for cell fate selection in a population of genetically identical cells. (A) Variation during infection (for example, spontaneous chemical kinetic noise) leads to qualitative differences in cell fate. (B) Variation in the physical state of individual cells before infection predetermines cell fate.

tions of the individual molecular components of phage lambda are not sufficient to explain such system-level behavior. Second, Arkin and colleagues (7) mapped the process of cell fate selection onto an explicit model of intracellular physics, which forces a recognition of the fact that many systems in biology are composed of components whose cellular abundances are far below levels for which continuous approximations of chemical kinetics are valid (11) and for which precision of behavior cannot be expected to emerge via the bulk averaging of many individual reaction events (12).

The Arkin model also makes a strong claim—that cell fate differences in lambda-infected *Escherichia coli* are due to spontaneous biochemical noise during infection (Fig. 1A). However, to our knowledge, no experiments have been carried out to test

Author contributions: F.S.-P. and D.E. designed research; F.S.-P. performed research; F.S.-P. contributed new reagents/analytical tools; F.S.-P. and D.E. analyzed data; and F.S.-P. and D.E. wrote the paper.

The authors declare no conflict of interest.

This article is a PNAS Direct Submission.

Freely available online through the PNAS open access option.

¹To whom correspondence should be addressed at: Department of Bioengineering, Stanford University, Stanford, CA 94305. E-mail: endy@stanford.edu.

This article contains supporting information online at www.pnas.org/cgi/content/full/0808831105/DCSupplemental.

© 2008 by The National Academy of Sciences of the USA

space, then the refractive index in the corresponding direction in physical space is n . Figure 2 as well as calculations (21) show that the ratio of the line elements is neither infinite nor zero. Even at a branch point the spatial deformation in any direction is finite, because here the coordinate grid is only compressed in angular direction by a finite factor, in contrast to optical conformal mapping (9). Furthermore, the spatial deformations are gradual, for avoiding reflections at boundaries (23).

Figure 3 illustrates the extension of our idea to three dimensions. Instead of the 2D surface of the globe of Fig. 2A, we use the 3D surface of a 4D sphere (a hypersphere). Such a geometry is realized (24, 25) in Maxwell's fish eye (1, 26). Inside the cloaking device, we inflate a 2D surface, the branch cut in 3D, like a balloon to make space for the 3D surface of the hypersphere. Again, at this point the cloak is invisible but does not hide anything yet. Then we open another spatial branch on the "zip" of the hypersphere to create a hidden interior. The branch cuts are curved surfaces in electromagnetic space, which is the only important difference when compared with the 2D case. Some light rays may pierce the entrance to the hypersphere twice; they perform two loops in the non-Euclidean branch. In physical space, light is wrapped around the invisible interior in such cases (Fig. 3B). We calculated

the required electromagnetic properties (21) and found that the electric permittivity ranges from 0.28 to 31.2 for our specific example. One could give the cloaking device any desired shape by further coordinate transformations, which would change the requirements on the optical properties of the material. As a rule, the larger the cloaked fraction of the total volume of the device, the stronger the optics of the material must be, but the required speed of light will always remain finite.

References and Notes

- M. Born, E. Wolf, *Principles of Optics* (Cambridge Univ. Press, Cambridge, 1999).
- U. Leonhardt, T. G. Philbin, *New J. Phys.* **8**, 247 (2006).
- U. Leonhardt, T. G. Philbin, in press; preprint available at <http://arxiv.org/abs/0805.4778> (2008).
- V. M. Shalaev, *Science* **322**, 384 (2008).
- D. Schurig *et al.*, *Science* **314**, 977 (2006), published online 18 October 2006; 10.1126/science.1133628.
- An early precursor of transformation optics is (7).
- L. S. Dolin, *Izvestiya Vusov* **4**, 964 (1961).
- A. Greenleaf, M. Lassas, G. Uhlmann, *Math. Res. Lett.* **10**, 1 (2003).
- U. Leonhardt, *Science* **312**, 1777 (2006), published online 24 May 2006; 10.1126/science.1126493.
- J. B. Pendry, D. Schurig, D. R. Smith, *Science* **312**, 1780 (2006), published online 24 May 2006; 10.1126/science.1125907.
- J. Yao *et al.*, *Science* **321**, 930 (2008).
- J. Valentine *et al.*, *Nature* **455**, 376 (2008).
- J. B. Pendry, *Science* **322**, 71 (2008), published online 28 August 2008; 10.1126/science.1162087.

- T. G. Philbin *et al.*, *Science* **319**, 1367 (2008).
- A. Greenleaf, Y. Kurylev, M. Lassas, G. Uhlmann, *Phys. Rev. Lett.* **99**, 183901 (2007).
- G. W. Milton, *The Theory of Composites* (Cambridge Univ. Press, Cambridge, 2002).
- D. R. Smith, J. B. Pendry, M. C. K. Wiltshire, *Science* **305**, 788 (2004).
- C. M. Soukoulis, S. Linden, M. Wegener, *Science* **315**, 47 (2007).
- A. K. Sarychev, V. M. Shalaev, *Electrodynamics of Metamaterials* (World Scientific, Singapore, 2007).
- H. Chen, C. T. Chan, *J. Appl. Phys.* **104**, 033113 (2008).
- See the supporting material on Science Online.
- U. Leonhardt, *New J. Phys.* **8**, 118 (2006).
- W. S. Cai, U. K. Chettiar, A. V. Kildishev, V. M. Shalaev, G. W. Milton, *Appl. Phys. Lett.* **91**, 111105 (2007).
- R. K. Luneburg, *Mathematical Theory of Optics* (Univ. of California Press, Berkeley, CA, 1964).
- H. A. Buchdahl, *Am. J. Phys.* **46**, 840 (1978).
- J. C. Maxwell, *Cambridge Dublin Math. J.* **8**, 188 (1854).
- We thank N. V. Korolkova for her generous support of this work. We are grateful for funding from European Union Contract Computing with Mesoscopic Photonic and Atomic States, the grants MSM0021622409 and MSM0021622419, and a Royal Society Wolfson Research Merit Award.

Supporting Online Material

www.sciencemag.org/cgi/content/full/1166332/DC1

SOM Text

Figs. S1 to S15

References

23 September 2008; accepted 5 November 2008

Published online 20 November 2008;

10.1126/science.1166332

Include this information when citing this paper.

Control of Self-Assembly of DNA Tubules Through Integration of Gold Nanoparticles

Jaswinder Sharma,^{1,2*} Rahul Chhabra,^{1,2*} Anchi Cheng,³ Jonathan Brownell,³ Yan Liu,^{1,2,†} Hao Yan^{1,2,†}

The assembly of nanoparticles into three-dimensional (3D) architectures could allow for greater control of the interactions between these particles or with molecules. DNA tubes are known to form through either self-association of multi-helix DNA bundle structures or closing up of 2D DNA tile lattices. By the attachment of single-stranded DNA to gold nanoparticles, nanotubes of various 3D architectures can form, ranging in shape from stacked rings to single spirals, double spirals, and nested spirals. The nanoparticles are active elements that control the preference for specific tube conformations through size-dependent steric repulsion effects. For example, we can control the tube assembly to favor stacked-ring structures using 10-nanometer gold nanoparticles. Electron tomography revealed a left-handed chirality in the spiral tubes, double-wall tube features, and conformational transitions between tubes.

Nanoparticles can exhibit distinctive electronic, magnetic, and photonic properties (1), and their assembly into well-defined

one-dimensional (1D), 2D, and 3D architectures with geometric controls could add to their functionality. DNA-mediated assembly of nanoparticles is an attractive way to organize both metallic and semiconducting nanoparticles into periodic or discrete 1D and 2D structures (1–14) through the programmable base-pairing interactions and the ability to construct branched DNA nanostructures of various geometries. Recent success in using DNA as a molecular glue to direct gold nanoparticles (AuNPs) into periodic 3D crystalline lattices further demonstrates the

power of DNA as building blocks for 3D nano-engineering (15, 16).

Here, we report a group of complex 3D geometric architectures of AuNPs created using DNA tile-mediated self-assembly. These are tubular nanostructures with various conformations and chiralities resembling those of carbon nanotubes. The nanoparticle tube assembly can be engineered both by the underlying DNA tile scaffolds and the nanoparticles themselves. Previous work in structural DNA nanotechnology has shown that DNA tubes can form through either the self-association of multi-helix DNA bundle structures or the closing up of 2D DNA tile lattices (17–26). The forces that drive tube formation have been attributed to the intrinsic curvature of the tile-array (21) and the thermodynamic requirement to lower the free energy of the system by minimizing the number of unpaired sticky ends (22). The intrinsic dimensional anisotropy of the DNA tiles also plays an important role in the kinetic control of the tube growth (26).

In all of the above studies, the true 3D conformations of DNA tubes have never been revealed in detail because of limitations in microscopic imaging techniques; deposition of the samples on a surface for atomic force microscope (AFM) or transmission electron microscope (TEM) imaging usually causes flattening and sometimes opening of the tubes. This limitation has prevented a comprehensive understanding of the structural features of DNA nanotubes. For example, the handedness of the chiral tubes can be better revealed with 3D structural characteriza-

¹Center for Single Molecule Biophysics, The Biodesign Institute, Arizona State University, Tempe, AZ 85287, USA.

²Department of Chemistry and Biochemistry, Arizona State University, Tempe, AZ 85287, USA. ³National Resource for Automated Molecular Microscopy, The Scripps Research Institute, La Jolla, CA 92037, USA.

*These authors contributed equally to this work.

†To whom correspondence should be addressed. E-mail: hao.yan@asu.edu (H.Y.); yan_liu@asu.edu (Y.L.)

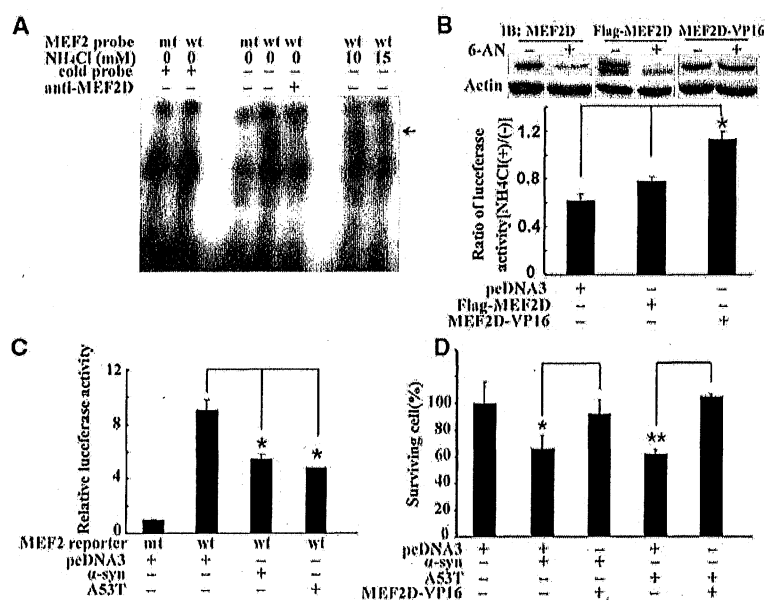


Fig. 4. Impairment of MEF2 function and neuronal survival after blockade of CMA. (A) Inhibition of MEF2D DNA binding activity by NH₄Cl. MEF2D DNA binding activity in SN4741 cells was assessed by EMSA after NH₄Cl treatment (arrow indicates the specific MEF2D-probe complex). (B) Effect of enhanced nuclear MEF2D on NH₄Cl-mediated inhibition. Levels of endogenous and transfected MEF2D in the nucleus (top panel) and MEF2 reporter activities (lower graph) in SN4741 cells were determined after 6-AN or NH₄Cl treatment, respectively (n = 3, *P < 0.05). (C) Inhibition of MEF2 transactivation activity by α-synuclein. MEF2 reporter gene expression was measured after 36 hours of overexpression of wild-type or A53T α-synuclein in SN4741 cells (n = 4, *P < 0.05). (D) Effect of increasing nuclear MEF2D function on α-synuclein-induced neuronal death. The viability of SN4741 cells was determined by WST assay after overexpression of indicated proteins (mean ± SEM, n = 4; *P < 0.05, **P < 0.01).

in neuronal viability (Fig. 4D). Coexpression of MEF2D-VP16 protected the cells against α-synuclein toxicity.

Our studies link CMA directly to the nuclear survival machinery. Because only α-synuclein mutants block substrate uptake in CMA (18), it has been unclear why an increase in the level of wild-type α-synuclein causes PD (23). Our findings that α-synuclein disrupts CMA-mediated degradation of MEF2D at a step prior to substrate uptake explain the toxic effects of both wild-type and mutant α-synuclein. Expression of Hsc70 suppresses α-synuclein toxicity in a *Drosophila* model of PD (24), consistent with our finding that maintenance of MEF2 function attenuates α-synuclein-induced neuronal death. Blocking CMA is accompanied by a clear decline of MEF2 function. Because the accumulated MEF2D binds poorly to DNA, the finding that the accumulated MEF2D binds poorly to DNA suggests important mechanisms in addition to nuclear export for the control of MEF2 activity. MEF2s play diverse roles in non-neuronal systems under physiological and pathological conditions (25). Our findings raise the possibility that degradation of MEF2s by CMA may function in other processes.

References and Notes

- Z. Mao, A. Bonni, F. Xia, M. Nadal-Vicens, M. E. Greenberg, *Science* 286, 785 (1999).
- X. Gong et al., *Neuron* 38, 33 (2003).
- P. Gonzalez et al., *Neurosci. Lett.* 411, 47 (2007).

- P. D. Smith et al., *J. Neurosci.* 26, 440 (2006).
- X. Tang et al., *J. Neurosci.* 25, 4823 (2005).
- J. F. Dice, *Autophagy* 3, 295 (2007).
- R. A. Nixon, *Trends Neurosci.* 29, 528 (2006).
- D. C. Rubinsztein, *Nature* 443, 780 (2006).

- U. Bandhyopadhyay, A. M. Cuervo, *Exp. Gerontol.* 42, 120 (2007).
- J. H. Son et al., *J. Neurosci.* 19, 10 (1999).
- P. Saftig et al., *EMBO J.* 14, 3599 (1995).
- H. S. Chun et al., *J. Neurochem.* 76, 1010 (2001).
- A. M. Cuervo, E. Knecht, S. R. Terlecky, J. F. Dice, *Am. J. Physiol.* 269, C1200 (1995).
- A. Massey, R. Kiffin, A. M. Cuervo, *Int. J. Biochem. Cell Biol.* 36, 2420 (2004).
- P. F. Finn, N. T. Mesires, M. Vine, J. F. Dice, *Autophagy* 1, 141 (2005).
- P. O. Seglen, P. B. Gordon, *Proc. Natl. Acad. Sci. U.S.A.* 79, 1889 (1982).
- A. E. Majeski, J. F. Dice, *Int. J. Biochem. Cell Biol.* 36, 2435 (2004).
- A. M. Cuervo, L. Stefanis, R. Fredenburg, P. T. Lansbury, D. Sulzer, *Science* 305, 1292 (2004).
- J. L. Webb, B. Ravikumar, J. Atkins, J. N. Skepper, D. C. Rubinsztein, *J. Biol. Chem.* 278, 25009 (2003).
- L. J. Martin et al., *J. Neurosci.* 26, 41 (2006).
- Z. Mao, M. Wiedmann, *J. Biol. Chem.* 274, 31102 (1999).
- H. P. Bogerd, R. A. Fridell, R. E. Benson, J. Hua, B. R. Cullen, *Mol. Cell. Biol.* 16, 4207 (1996).
- A. B. Singleton et al., *Science* 302, 841 (2003).
- P. K. Auluck, H. Y. E. Chan, J. Q. Trojanowski, V. M.-Y. Lee, N. M. Bonini, *Science* 295, 865 (2002); published online 20 December 2001 (10.1126/science.1067389).
- M. P. Czubryt, E. N. Olson, *Recent Prog. Horm. Res.* 59, 105 (2004).
- We thank H. Rees and D. Cooper at Emory Neuroscience NINDS Core Facility (NS055077) and UAB Neuroscience Core Facility (NS47466 and NS57098) for assistance in imaging and immunohistochemistry analysis, and J. Blum and A. M. Cuervo for Hsc70 and Lamp2a constructs. Supported by NIH grants NS048254 (Z.M.), AG023695 (Z.M.), and NS038065 (M.L.) and by Emory and UAB Alzheimer's Disease Research Center pilot grants (Z.M. and J.J.S.) and the Robert Woodruff Health Sciences Center Fund (Z.M.).

Supporting Online Material

www.sciencemag.org/cgi/content/full/323/5910/124/DC1
Materials and Methods
Figs. S1 to S9
References

18 September 2008; accepted 5 November 2008
10.1126/science.1166088

Signal Sequences Activate the Catalytic Switch of SRP RNA

Niels Bradshaw,* Saskia B. Neher,* David S. Booth, Peter Walter†

The signal recognition particle (SRP) recognizes polypeptide chains bearing a signal sequence as they emerge from the ribosome, and then binds its membrane-associated receptor (SR), thereby delivering the ribosome-nascent chain complex to the endoplasmic reticulum in eukaryotic cells and the plasma membrane in prokaryotic cells. SRP RNA catalytically accelerates the interaction of SRP and SR, which stimulates their guanosine triphosphatase (GTPase) activities, leading to dissociation of the complex. We found that although the catalytic activity of SRP RNA appeared to be constitutive, SRP RNA accelerated complex formation only when SRP was bound to a signal sequence. This crucial control step was obscured because a detergent commonly included in the reaction buffer acted as a signal peptide mimic. Thus, SRP RNA is a molecular switch that renders the SRP-SR GTPase engine responsive to signal peptide recruitment, coupling GTP hydrolysis to productive protein targeting.

Secretory and transmembrane proteins are delivered to the membrane cotranslationally by the signal recognition particle (SRP) and its membrane-associated receptor (SR) (1).

SRP recognizes signal sequences as they emerge from the ribosome (2) and then associates with SR at the membrane where the ribosome is transferred to the translocon. The guanosine triphos-

(Fig. 4A). VopSA30 did not modify DA-Rac-T35A, confirming that the AMP modification is specific for Thr³⁵ (Fig. 4A). As expected, DA-Rac incubated with VopS-H348A was not modified (Fig. 4A). To confirm that VopS modifies other members of the Rho family GTPases, we repeated the *in vitro* labeling assay using Rho, Rac, and Cdc42. In the presence of VopS, all of the GTPases were modified with AMP, whereas they were not modified in the presence of ³²P- α -labeled ATP alone or by VopS-H348A (Fig. 4B). Thus, VopS modifies Rho GTPases with AMP. We now refer to this activity as AMPylation and the enzyme as an AMPylator. VopS uses this posttranslational modification of AMPylation to hinder signaling between Rho GTPases and their downstream effectors by blocking the effector binding site on the switch I region of the GTPase with AMP.

Both VopS and protein kinases use ATP to modify substrates, but the phosphate attached to the substrate is distinct. Kinases use the γ phosphate of ATP to modify their substrates on tyrosine, threonine, and serine residues, whereas VopS uses the α phosphate linked to adenosine to modify its substrate on a threonine residue. This type of posttranslational modification on eukaryotic proteins has not previously been observed. However, it has been observed for bacterial glutamine synthetase, albeit autocatalytically on a tyrosine residue, resulting in the sensitization of end-product inhibition (13, 14). Because bacterial type III secreted effectors often mimic eukaryotic mechanisms, the observation of AMPylation by a bacterial effector prompted us to investigate whether eukaryotes use this posttranslational modification. Incubation of S100 HeLa cell lysates with ³²P- γ -labeled ATP predictably revealed many phosphorylated protein substrates (Fig. 4C). This modification, phosphorylation, was labile in the presence of a phosphatase (Fig. 4C). To test whether the same type of experiment would reveal AMPylated protein substrates, we incubated S100 lysate with ³²P- α -labeled ATP. A number of radiolabeled proteins were observed but were insensitive to phosphatase treatment (Fig. 4C). The addition of purified recombinant VopSA30 to the reaction using ³²P- α -labeled ATP, but not ³²P- γ -labeled ATP, specifically increased labeling at the predicted size of the Rho GTPases (Fig. 4C). Thus, VopS is not a promiscuous AMPylator but rather targets the Rho family of GTPases. Consistent with this observation, phosphorylation and AMPylation did not occur in the presence of denatured protein (Fig. 4C). Thus, eukaryotic proteins can use ATP to modify proteins by AMPylation.

VopS contains a C-terminal Fic domain, and mutation of an invariant histidine residue within this domain led to the discovery of the catalytic activity of modifying proteins with AMP. The conserved histidine is critical for the AMPylation activity. The limited eukaryotic distribution of Fic resembles that of other components of signal transduction machinery and might support a role for AMPylation by eukaryotic Fic domains in signaling. Structures of Fic domains place the con-

served polar residues of this motif within a cleft that could represent an active site, with conserved side chains (from E and N) forming polar contacts with a phosphate in one structure (fig. S3A) (15). A β hairpin located near the motif binds peptide in another structure, placing a side chain of the peptide within van der Waals contact of the motif histidine (fig. S3B). Although enzymes, such as an activated E1, form AMP-bound covalent enzyme intermediates to drive chemical ligation reactions (16), AMP has not previously been shown to be used as a stable posttranslational modification for a protein. This activity represents an ideal posttranslational modification because it (i) uses a highly abundant high-energy substrate, ATP; (ii) results in the formation of a reversible phosphodiester bond; (iii) is bulky enough to bind to an adaptor protein and be used in dynamic multidomain signaling complexes; and (iv) alters the activity of the protein it modifies. It is intriguing that we observed this modification on threonine because this residue is used in many other modifications that might compete with AMPylation. The identification of the substrates and enzymes involved in eukaryotic AMPylation will undoubtedly add a new layer to the expanding complexity of our information about cellular signal transduction.

References and Notes

1. N. A. Daniels *et al.*, *J. Infect. Dis.* **181**, 1661 (2000).
2. K. Makino *et al.*, *Lancet* **361**, 743 (2003).
3. K. S. Park *et al.*, *Microbiol. Immunol.* **48**, 313 (2004).
4. P. Ghosh, *Microbiol. Mol. Biol. Rev.* **68**, 771 (2004).
5. D. L. Burdette, M. L. Yarbrough, A. Orvedahl, C. J. Gilpin, K. Orth, *Proc. Natl. Acad. Sci. U.S.A.* **105**, 12497 (2008).
6. T. Casselli, T. Lynch, C. M. Southward, B. W. Jones, R. DeVinney, *Infect. Immun.* **76**, 2202 (2008).

7. K. S. Park *et al.*, *Infect. Immun.* **72**, 6659 (2004).
8. Single-letter abbreviations for the amino acid residues are as follows: A, Ala; C, Cys; D, Asp; E, Glu; F, Phe; G, Gly; H, His; I, Ile; K, Lys; L, Leu; M, Met; N, Asn; P, Pro; Q, Gln; R, Arg; S, Ser; T, Thr; V, Val; W, Trp; X, any amino acid; and Y, Tyr.
9. R. Utsumi, Y. Nakamoto, M. Kawamukai, M. Himeno, T. Komano, *J. Bacteriol.* **151**, 807 (1982).
10. T. Hakoshima, T. Shimizu, R. Maesaki, *J. Biochem.* **134**, 327 (2003).
11. J. B. Bliska, K. L. Guan, J. E. Dixon, S. Falkow, *Proc. Natl. Acad. Sci. U.S.A.* **88**, 1187 (1991).
12. N. Abdul-Manan *et al.*, *Nature* **399**, 379 (1999).
13. P. B. Chock, S. G. Rhee, E. R. Stadtman, *Annu. Rev. Biochem.* **49**, 813 (1980).
14. M. S. Brown, A. Segal, E. R. Stadtman, *Proc. Natl. Acad. Sci. U.S.A.* **68**, 2949 (1971).
15. M. E. Cuff *et al.*, Midwest Center for Structural Genomics; structure has been deposited in the Protein Data Bank (www.rcsb.org) with the identification number 2F65.
16. A. L. Haas, J. V. Warms, I. A. Rose, *Biochemistry* **22**, 4388 (1983).
17. We thank N. Alto, R. Taussig, P. Sternweis, S. Mukherjee, M. Rosen, E. Olson, J. Goldstein, M. Brown, T. Iida, T. Honda, L. McCarter, and the Orth lab for insightful discussions, critical reading, and/or generous supply of reagents. K.O. and M.L.Y. are supported by grants from NIH—Allergy and Infectious Disease (R01-AI056404) and the Welch Foundation (I-1561). L.N.K. and N.G. are supported by the Welch Foundation (I-1505) and Howard Hughes Medical Institute. K.O. is a Beckman Young Investigator, Burroughs Wellcome Investigator, and W. W. Caruth Biomedical Scholar.

Supporting Online Material

www.sciencemag.org/cgi/content/full/1166382/DC1
Materials and Methods
Figs. S1 to S3
References

25 September 2008; accepted 14 November 2008
Published online 27 November 2008;
10.1126/science.1166382
Include this information when citing this paper.

Simpson's Paradox in a Synthetic Microbial System

John S. Chuang,* Olivier Rivoire, Stanislas Leibler

The maintenance of "public" or "common good" producers is a major question in the evolution of cooperation. Because nonproducers benefit from the shared resource without bearing its cost of production, they may proliferate faster than producers. We established a synthetic microbial system consisting of two *Escherichia coli* strains of common-good producers and nonproducers. Depending on the population structure, which was varied by forming groups with different initial compositions, an apparently paradoxical situation could be attained in which nonproducers grew faster within each group, yet producers increased overall. We show that a simple way to generate the variance required for this effect is through stochastic fluctuations via population bottlenecks. The synthetic approach described here thus provides a way to study generic mechanisms of natural selection.

A simple general principle has emerged from theoretical and experimental studies of common-good producer–nonproducer interactions: For producers to be selected and maintained, they have to be the privileged recipients of the common good (1–18). Producers may become privileged recipients by virtue of kinship or spatial proximity or discrimination through reciprocity or some distinctive feature (1–5, 9, 10, 14).

In this work, we considered the scenario in which producers and nonproducers are distributed heterogeneously into subpopulations of varying composition, some starting with higher

Center for Studies in Physics and Biology and Laboratory of Living Matter, The Rockefeller University, 1230 York Avenue, New York, NY 10065, USA.

*To whom correspondence should be addressed. E-mail: chuangj@rockefeller.edu